










RESEARCH ARTICLE

Geochemical and microbial responses to limestone and peat treatment of incubated hypermonosulfidic sediments

Liubov Kononova¹  | Anders Johnson²  | Sten Engblom³  | Pekka Stén⁴ |
Changxun Yu¹  | Peter Österholm⁵ | Vadim Kessler⁶  |
Gulaim Seisenbaeva⁶  | Mark Dopson²  | Mats Åström¹  |
Eva Högfors-Rönnholm³ 

¹Biology and Environmental Sciences, Linnaeus University, Kalmar, Sweden

²Centre for Ecology and Evolution in Microbial Model Systems (EEMiS), Linnaeus University, Kalmar, Sweden

³Research and Development, Novia University of Applied Sciences, Vaasa, Finland

⁴Environmental Technology, Vaasa University of Applied Sciences, Vaasa, Finland

⁵Department of Geology and Mineralogy, Åbo Akademi University, Åbo, Finland

⁶Department of Molecular Sciences, BioCenter Swedish University of Agricultural Sciences, Uppsala, Sweden

Correspondence

Liubov Kononova, Biology and Environmental Sciences, Linnaeus University, SE-39231 Kalmar, Sweden.
Email: liubov.kononova@lnu.se

Funding information

European Regional Development Fund; Maa- ja Vesitekniikan Tuki Ry, Grant/Award Number: 45971; Science for Life Laboratory (SciLifeLab); National Genomics Infrastructure (NGI); Swedish Research Council, Grant/Award Numbers: 2022-06725, 2018-05973

Abstract

Fine-grained hypermonosulfidic sediments are widespread on the coastal plains of the northern Baltic Sea that when drained, cause the formation and dispersion of acid and toxic-metal species. In this study, a 30-month laboratory oxidation experiment with such a sediment was performed in incubation cells. To minimize or prevent acidification, limestone was applied in two grain sizes: agricultural limestone with particles that were all <3.15 mm and half of them <0.80 mm, and fine-grained limestone with a median grain size of 2.5 µm. The amount of limestone applied corresponded to the theoretical acidity contained in the sulfides, as well as four times that amount. Another treatment included addition of peat to the low limestone dose to test its effects on immobilizing sulfur and metals. The pH of the drainage water and solid phase decreased to pH <4.0 in the control, and to pH <5.0 in the coarse-grained low-limestone treatment, but remained near-neutral in the other treatments. Hence, the fine-grained limestone effectively hindered acidity formation in contrast with the coarse-grained limestone when applied in amounts corresponding to the potential acidity held in the sulfides. The limestone treatments further overall decreased the rate of pyrite oxidation, slowed down the movement of the oxidation front, strongly minimized the formation of dissolved and solid-phase labile Al, and caused formation of gypsum as well as more labile secondary Fe(III) phases than corresponding Fe phases formed in the control. The limestone and peat treatments also caused shifts in the 16S rRNA gene-based microbial communities, where the control developed acidophilic iron and sulfur oxidizing communities that promoted acidity and metal release. Instead, the limestone-treated unacidified incubations developed acid tolerance to neutrophilic communities of iron and sulfur oxidizers that promoted sulfate formation without acidity release. The results showed that limestone treatments

Liubov Kononova and Anders Johnson shared first authorship.

This is an open access article under the terms of the [Creative Commons Attribution](https://creativecommons.org/licenses/by/4.0/) License, which permits use, distribution and reproduction in any medium, provided the original work is properly cited.

© 2024 The Author(s). *European Journal of Soil Science* published by John Wiley & Sons Ltd on behalf of British Society of Soil Science.

have several biogeochemical effects, and that using a fine-grained limestone as amendment was favourable in terms of minimizing acidity formation and metal release.

KEYWORDS

acidity, iron monosulfides, limestone, sediments, sulfur, treatments

1 | INTRODUCTION

Metastable iron sulfides, which are generally defined by dissolution in acid and thus called ‘acid volatile sulfide’ (Rickard & Morse, 2005), are thermodynamically unstable relative to pyrite (FeS_2), but despite this, can persist in large quantities over geological time scales. Such a situation occurs on the coastal plains of the Gulf of Bothnia where fine-grained sediments containing metastable iron sulfides and/or pyrite cover up to 10,000 km^2 in Finland (Edén et al., 2023) and an area probably of similar size in Sweden (Nyman et al., 2023). Although studies are few, it seems like the most common situation is co-occurrence of the minerals (Boman et al., 2008, 2010). These sediments were formed under reducing conditions in shallow waters of the Baltic Sea during Holocene. Owing to isostatic land uplift following the melting of the Weichselian ice sheet in the late Pleistocene, they are now found in the terrestrial landscape. The mineralogy and chemistry of the metastable iron sulfides in these sediments are poorly known, with the few existing analyses showing disseminated fine-grained ($<30 \mu\text{m}$) crystals with an average elemental composition of $\text{FeS}_{1.1}$ indicative of a mixture of mackinawite and greigite (Boman et al., 2008). A possible reason as to why these minerals have been preserved in large quantities is that a combination of low availability of sulfate due to brackish water conditions and high availability of Fe due to unusually high Fe concentrations in incoming rivers and creeks (Salminen et al., 2005) result in aqueous and sedimentary settings with high Fe to S ratios favouring monosulfides (Boesen & Postma, 1988). This hypothesis is supported by the strong dominance of acid-volatile sulfide relative to pyrite along with a large pool of non-sulfidized Fe(II) in recent estuarine sediments in the region (Yu et al., 2015).

Severe environmental problems arise when the sulfide-rich sediments around the Gulf of Bothnia are artificially drained and disturbed. This occurs via (i) large networks of open and subsurface drains to allow for agricultural cultivation, (ii) excavation and removal during infrastructure and urban development as the sediments have poor geotechnical properties, and (iii) dredging in shallow water estuaries and near coastal areas. The direct impact of these activities is the formation of highly acidic soils, referred to as acid sulfate

Highlights

- Fine-grained limestone effectively prevents acidification of oxidizing hypermonosulfidic sediment.
- Adding limestone to oxidizing hypermonosulfidic sediment decelerate pyrite oxidation and suppress the redox.
- Adding peat, in addition to limestone, to oxidizing hypermonosulfidic sediment causes a decline in pH and Fe retention.
- Maintenance of high pH hinders development of acidophilic microbial taxa, but not neutrophilic iron and sulfur oxidizers.

soils, with typical far-reaching off-site environmental effects. These effects include acidification and metal contamination of surface waters (Edén et al., 1999; Joukainen & Yli-Halla, 2003; Lindgren et al., 2022) with associated ecological deterioration (Toivonen et al., 2020) and metal pollution of estuarine settings (Åström et al., 2012; Nordmyr et al., 2008; Yu, Turner, et al., 2024) as well as sea sediments (Virtasalo et al., 2020). Attempts to neutralize the agricultural acid sulfate soils via various liming strategies (Åström et al., 2007; Björkqvist & Weppling, 1987) and hydrological controls (Bärlund et al., 2005; Österholm et al., 2015) have so far more or less failed on a regional scale. Furthermore, a recent example of liming of disposed dredged masses failed as the pH dropped to 3.0 (Johnson et al., 2022). Laboratory-based experiments measuring physicochemical variables before and after a defined period of oxidation have provided some insight into the general mechanisms of acidity formation and metal release when these sediments are oxidized (Åström & Björklund, 1997; Kronberg et al., 2024; Mattbäck et al., 2022; Peltola & Åström, 2002). However, there is no knowledge on how the formation of acidity and metal release develops over time, and how liming in various doses and grain sizes can prevent development of environmentally unfriendly soil conditions.

Acidophilic microorganisms have long been known to inhabit acid sulfate soil settings. For example, Wiklander et al. (1950) described that the sulfur oxidation

reaction 'is both of a chemical and biological nature'. Later, *Acidithiobacillus* spp. were identified in these soils (Arkesteyn, 1980) as well as *Acidithiobacillus* genus cell numbers were shown to correlate to metal and acid discharge from the soils (Niemela & Tuovinen, 1972). It is now known that acidophiles are responsible for a major part of the oxidation pathway whereby metal sulfides in acid sulfate soils are converted to ferric-iron compounds and sulfuric acid. They survive in acidic (Slonczewski et al., 2009), with an optimum pH below 5 (for extreme acidophiles pH < 3), and metal-laden conditions by a combination of biotic systems and abiotic complexation of the free metal by sulfate ions (Dopson et al., 2014). In sulfidic sediments around the Gulf of Bothnia that have been rapidly oxidized, extreme acidophiles such as *Acidocella* and *Acidithiobacillus* spp. were identified in laboratory reactors (Wu et al., 2013) and *Acidithiobacillus* spp. and other biomineral-associated taxa in a field setting (Johnson et al., 2022). In contrast, older and more established acid sulfate soils tend to be dominated by iron and sulfur oxidizing moderate acidophiles like *Gallionella* and *Sulfuricella* (Christel et al., 2019; Högfors-Rönholm et al., 2022; Wu et al., 2013). However, only a few studies have investigated how the microbial community responds and develops in pyrite and metastable iron-sulfide-containing sediments brought into the oxidation zone and concomitantly limed in order to keep the pH near neutral (Högfors-Rönholm et al., 2020, 2022). Furthermore, no studies focus on the plains on the eastern side of the Gulf of Bothnia or changes as the oxidation proceeds over an extended time. As previously shown, extreme acidophiles would be expected under unlimed conditions as severe acidity develops, but it is unknown which species will contribute to sulfide oxidation under limed conditions when the pH does not decrease.

The aim of this study was to determine the geochemical and microbial community evolution in a metastable iron-sulfide-containing sediment in the Gulf of Bothnia region when exposed to atmospheric oxygen in the laboratory. The experiment was designed to replicate the conditions that occur when these sediments are excavated and disposed of on land during land-use management. It included amendments in the form of various proportions and grain sizes of limestone to prevent acidification, as well as fine-grained peat to assess the impact of organic matter on sulfur and metal retention.

2 | MATERIALS AND METHODS

2.1 | Sediment excavation and the five treatments

A fine-grained (clay-silt) black sediment was excavated from well below the groundwater table at a site on the

coastal plains in Western Finland (63.04067° N, 21.74248° E). The sediment was massive without macropores and had very low hydraulic conductivity as defined for a similar sediment at a nearby site (Salo et al., 2023). The concentrations of total reduced sulfur (TRS) in three samples of the sediment were 0.48%, 0.52%, and 0.54% per dry weight (details in Section 3.1) and incubation gave a pH of <4.0 (details in Section 3.3). The sediment is thus defined as 'hypermonosulfidic' (Boman et al., 2023), and is the term that will be used here for the sediment in untreated and unoxidized form. Considering that one mole of sulfide produces two moles of acidity and one mole of CaCO₃ produces two moles of alkalinity, a 1:1 molar ratio of these two substances is the theoretical demand for neutralizing all sulfide-derived acidity by CaCO₃. For the lowest measured TRS value (0.48%), this corresponded to 10 kg limestone per m³ of the wet sediment. This amount of limestone was thus the main treatment option and included: (i) agricultural limestone (CaCO₃ with a Ca concentration of 37% and Mg concentrations of ≤2%) with particles that were all <3.15 mm, and half of them <0.80 mm (Aito Kalsiitti 'genuine calcite' by Nordkalk) referred to as L10_{3.15 mm}, (ii) fine-grained limestone with a median grain size of 2.5 μm (C2 quality by Nordkalk) referred to as L10_{2.5 μm}, and (iii) L10_{2.5 μm} plus fine-grained peat (milled to <20 μm; Vapo Fiber) referred to as PL10_{2.5 μm}. The peat had a biodegradation level of H1, which is the least decomposed fraction according to the von Post scale (Andriess, 1988). It typically contains 95%–98% organic carbon and 2%–5% inorganic carbon. The organic compounds include cellulose, hemicellulose, lignin, humic and fulvic acids, as well as extractives, waxes and resins. The non-organic content is represented by the ash residue after combustion. The peat was added due to its potential to bind released metals (Eberle et al., 2021), and as it may also work as a protective layer that decreases the oxidation rate of hypersulfidic materials (Nystrand et al., 2021). As not all limestone may be activated in the neutralization process (Hadzic et al., 2014) and the experiment was designed to ensure that one set of treatments maintained a high pH throughout the experiment (e.g., for determining outstanding microbial and chemical questions), four times the required theoretical limestone demand (40 kg/m³) was additionally used and included the coarse-grained and fine-grained limestone variant, referred to as L40_{3.15 mm} and L40_{2.5 μm}, respectively.

2.2 | Experimental setup and procedure

In the laboratory, immediately following the sampling, a mixer was used to homogenize 8 kg of the wet

hypermonosulfidic sediment (taken as a composite from the excavated sediment mass) with the required amount of limestone and in one case peat. After 2 min in the mixer, the sediment liquified, and after a further 2 min of mixing a homogeneous mixture of sediment and amendment was achieved. In the combined treatment with limestone and peat, the limestone was mixed in first. Thereafter, the sediment was placed into specially designed incubation cells. These cells consisted of opaque high-density polyethylene (HDPE) open boxes with a raised bottom in the form of a polypropylene (PP) grid to allow water to drain and accumulate in the 8-mm high space created. A drainage fabric between the sediment and the raised bottom stopped particles from entering the drainage space. A polyurethane (PU) tube in the drainage space was used for water sampling and drainage. The five treatments plus a control (only mixed) were prepared, all in triplicate, giving a set of 18 incubation cells that were randomized on a shelf to reduce the effect of any spatial variations in evaporation/temperature. The sediments were incubated at ambient laboratory temperature (19–21°C) for 30 months starting on 2 December 2019 and ending on 24 May 2022. The cells containing the sediment were irrigated with 1 L of ultrapure water once a week from the start of the experiment until December 2020, corresponding to a mean natural precipitation in the month of June during the last 4 years. After December 2020, the frequency of irrigation was halved (i.e., to biweekly) as was the water sampling, which meant that throughout the experiment an equal amount of water was added before sampling, but during the latter half of the experiment the period of possible evaporation was extended. After every water sampling, the cells were completely drained and thus dried out allowing cracks to be formed and oxygen to enter. As would be the case in a natural dredge spoil, water from subsequent irrigations followed the formed macropores and accumulated at the bottom. The sediment was in contact with the liquid phase through capillary rise, and also a water level that increased with every irrigation. Two cells were irrigated without sediment and showed no measurable effect of the materials used in the experiment.

2.3 | Drainage water

The added ultrapure water that had equilibrated with the sediment and perhaps particularly with the macropore surfaces (henceforth termed drainage water) was collected from the PU tube approximately monthly during the first year (December 2019–November 2020), and approximately bimonthly thereafter. This gave a total of 23 sampling

occasions and for each, the volume of drained water was registered. The amount of drained water volume varied widely, in a pattern that was similar for all 18 incubation cells with peaks from approximately the 6th to the 13th month (June–November 2020), and from approximately the 20th to the 27th month (June–December 2021) (Figure 1c). This corresponded to more humid conditions (and thus lower evaporation) in summer and autumn than in winter and spring. The total volume of drained water for the whole period was in ascending order: control (median: 16.2 L) < L40_{2.5} μm (19.4) < PL10_{2.5} μm (19.6) < L40_{3.15} mm (20.1) < L10_{3.15} mm (23.5) < L10_{2.5} μm (27.8).

The pH and Eh were determined as described in S11. The concentrations of Fe, Al, Si, Ca, Mg, K and Na were determined in filtered (0.45 μm) and acidified (HNO₃; pH < 1.8) samples by inductively coupled plasma (ICP) optical emission spectroscopy (ICP-OES), and ICP mass spectrometry (ICP-MS). Details of the analyses, including analytical precision and limit of quantification (LOQ) are given in Table S11. The concentrations of SO₄²⁻ and Cl⁻ were measured in filtered (0.45 μm) waters by ion chromatography (Dionex ICS 1100). The amounts of leached SO₄²⁻, Cl⁻, Si and metals were calculated by multiplying the concentration by water volume for each measurement separately and cumulatively over the entire period.

2.4 | Solid phase

2.4.1 | Sampling

Ten samples of the hypermonosulfidic sediment were collected prior to the application of the treatments. After 9 months, a small sample was taken by pressing a tube from the top to the bottom of the sediment. This sample thus represented the bulk of the sediment without consideration of the degree of oxidation. During the experiment, the hypermonosulfidic sediment developed physically. An aggregate structure having entrapped micropores and characterized by a greyish to brownish colour had formed (referred to as ‘aggregates’), and generally, a frequently brownish-stained layer had developed on top of the sediment and on crack surfaces (‘surface’). Furthermore, within interiors, the black massive character remained to various extent (‘residues’). The extent of these residues was estimated based on visual assessment made possible due to distinct differences in colour but shall be seen as indicative. At month 25, a sample was taken from each cell from the surface and aggregates, and, additionally, the residue wherever it occurred. For simplicity, and to make a distinction to the drainage waters, the solid-phase samples collected at months 0, 9 and 25 were referred to as start, mid and end sampling/

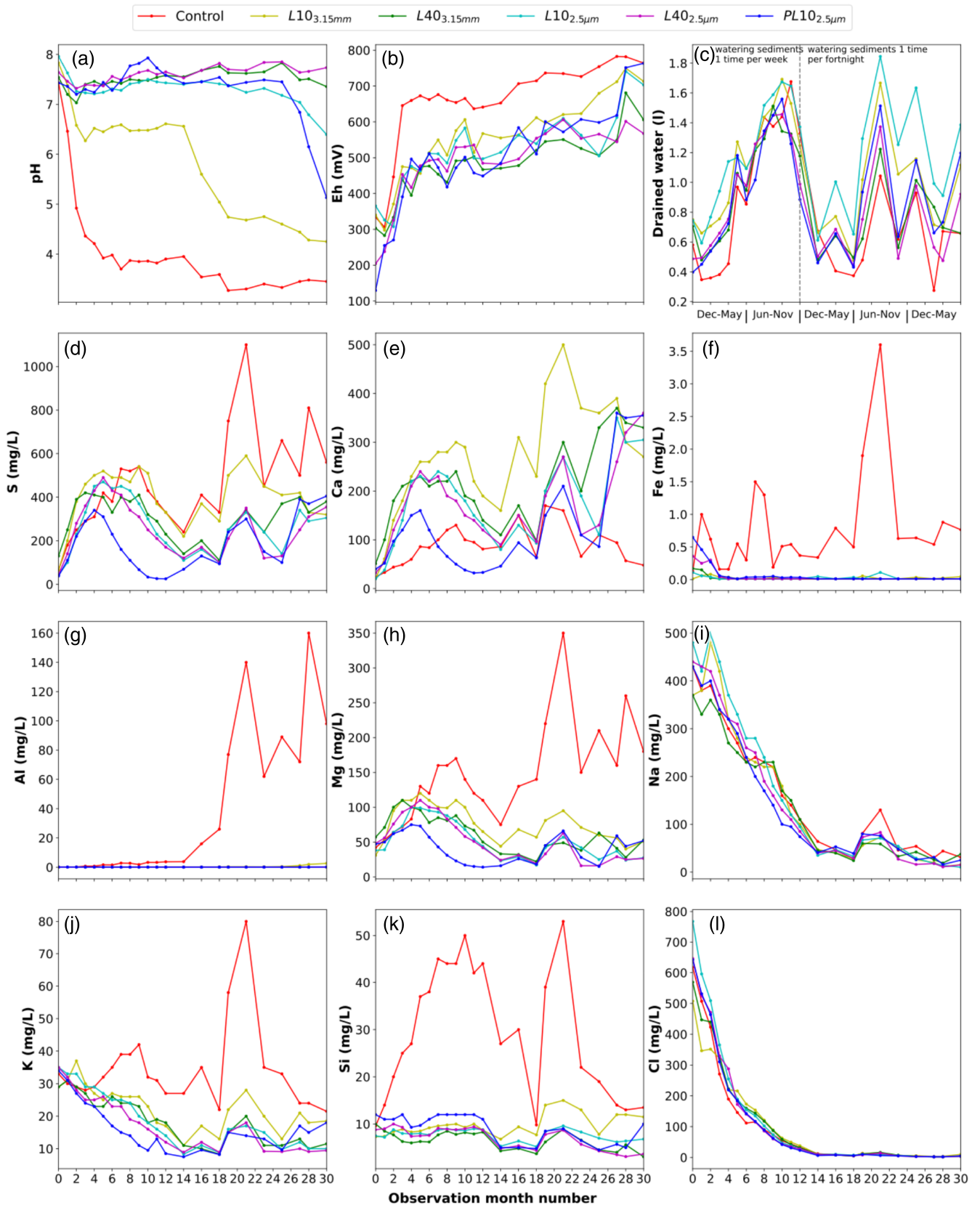


FIGURE 1 pH (a), Eh (b) the volume of water drained (c) and element concentrations (d-l) in water drained from the incubation cells including the control and the five treatments. The graphs represent median of triplicate incubation cells. The x-axis values refer to the month number after the start of the experiment in December 2019. Also shown (in c) is the change from weekly to biweekly watering and the month names.

samples, respectively. In addition, precipitates in the form of clearly visible crystals formed on the surface were picked by hand.

2.4.2 | pH, Eh, water content and LOI

The pH and Eh were determined as described in SI2. The water content of the wet sediment was determined by measuring the weight loss after drying at 105°C overnight (SFS-EN 12880). Loss on ignition (LOI), a rough estimate of the organic-matter concentration, was measured by the weight loss after igniting the dry samples at 550°C for 2.5 h (SFS-EN 12879).

2.4.3 | Total concentrations of S and metals

The total concentrations S, Fe, Al, Na, K, Ca and Mg were determined on freeze-dried samples by dissolution in a four-acid (HClO₄-HNO₃-HF-HCl) solution (Hall, Vaive, Beer, & Hoashi, 1996) followed by determination of S by ICP-OES and metals by ICP-MS. The analytical precision was estimated based on eight samples selected at random, prepared in duplicate, and analysed independently and anonymously (Gill, 1997). The precision was as follows: S 6.8%, Fe 1.8%, Al 2.1%, Ca 6.2%, Mg 3.8%, Na 2.7% and K 18%.

2.4.4 | Sulfur speciation

Sulfur speciation was performed according to a simplified distillation-based method for sulfidic soil materials (Dalhem et al., 2021). Briefly, acid-volatile sulfides (AVS) were extracted using 6 M HCl with 0.1 M ascorbic acid, while hot, chromium-reducible sulfur (CRS) was extracted using 3 M CrCl₂ by heating at 60°C. AVS is expected to dissolve minerals such as mackinawite and greigite and CRS pyrite plus elemental sulfur. The samples for this analysis were stored frozen and freeze-dried prior to analyses. All samples were run in duplicate, and the average result is presented.

2.4.5 | Sequential chemical extraction of metals

A three-step sequential chemical extraction (SCE) was carried out and including successively: (i) sodium acetate (CH₃COONa, pH 5.00, 1 h) referred to as NaOAc, that is specific for cations existing in solution, weakly bound (sorbed) to particle surfaces and trapped in carbonates (Lakanen & Erviö, 1971), (ii) tetrasodium pyrophosphate (0.1 M Na₄P₂O₇, alkaline conditions, 1 h) referred to as

TSPP that is specific for the labile organic component including humic and fulvic substances (Hall, 1998; Hall, Vaive, & MacLaurin, 1996); however, this reagent can to some extent release inorganic Fe due to peptization and dispersion of finely divided ferruginous particles (Hall, 1998; Jeanroy & Guillet, 1981), and (iii) hydroxylamine hydrochloride (0.25 M NH₂OH·HCl in 0.25 M HCl, pH < 2, 2 h, 60°C) referred to as HXL that specifically attacks poorly crystalline Fe and Mn oxyhydroxides (Hall, 1998; Hall, Vaive, Beer, & Hoashi, 1996) but also other acid-soluble minerals such as Al hydroxides and metastable iron sulfides.

The extracted solutions from each step were analysed for Fe, Al, Na, K, Ca and Mg by ICP-MS. The analytical precision was estimated based on eight samples selected at random, prepared in duplicate, and analysed independently and anonymously (Gill, 1997). The results are presented in Table SI2. A residual fraction was determined by difference: Residual fraction = C_{total} - (C_{NaOAc} + C_{TSPP} + C_{HXL}), where C stands for concentration.

2.4.6 | SEM-EDS, XRD and XAS

The precipitates (crystals) formed on the surface were analysed by Scanning Electron Microscopy with Energy Dispersive x-ray Spectroscopy (SEM-EDS) and x-ray diffraction (XRD). SEM micrographs of mineral powder materials were obtained using a Hitachi FlexSEM 1000II instrument with an acceleration voltage of 5 kV and a working distance of 5 mm. EDS spectra were obtained using an acceleration voltage of 20 kV and a working distance of 10 mm, applying Oxford Instruments AZtecOne hardware and software on the Hitachi FlexSEM 1000II instrument. For XRD, milled mineral powders were packed in 0.8 mm borosilicate glass capillaries. The diffraction patterns were recorded with a Bruker D8 Quest ECO multifunctional diffractometer using MoK α radiation with wavelength $\lambda = 0.71073 \text{ \AA}$, in PHI360 rotation mode with exposure times of 120 s for all samples. Integration of the 3D patterns and mineral identification were performed with DIFFRAC.EVA software, using the ICDD powder pattern database. Additionally, a sample of the surface of the control was analysed by Fe K-edge x-ray absorption spectroscopy to determine the Fe mineralogy (SI3).

2.4.7 | Microbiology

Samples (approximately 30 g) were aseptically collected with a sterile spoon, placed into a sterile 50 mL Falcon tube, and stored at 4°C until extraction the following day. DNA extractions, from 8 g of homogenized samples, followed an indirect extraction method (Högfors-Rönholm

et al., 2018). Briefly, samples were washed thrice with a sodium phosphate buffer to release intact cells from the sediment. Those cells were concentrated via centrifugation into a cell pellet, and the DNA from the resultant cell pellets was then extracted using the DNeasy PowerLyzer PowerSoil Kit (Qiagen) according to the manufacturer's instructions. The V3-V4 region of the 16S rRNA gene sequence was PCR amplified in a two-step technique to prepare a library and then sequenced as previously described (Högfors-Rönholm et al., 2020). The first PCR amplification used the 341F and 805R primer pair (Herlemann et al., 2011), and the second PCR attached unique Illumina sequencing tags to generate the final amplicons (2×300 bp pair-end reads; Hugerth et al., 2014). DNA quality and quantity were investigated by agarose gel electrophoresis, Qubit 2.0 Fluorometer (ThermoFisher), and TapeStation (Aligent # 4150). The amplicons library was sequenced at the Science for Life Laboratory, Sweden, on the Illumina MiSeq platform as previously described (Högfors-Rönholm et al., 2020).

Processing of the Illumina sequencing reads utilized the Ampliseq pipeline v1.2 (Straub et al., 2020), which incorporates QIIME2 (Bolyen et al., 2019) and DADA2 (Callahan et al., 2016), annotated against the SILVA database v138.1 (Quast et al., 2012) as previously described (Johnson et al., 2022). The 16S rRNA gene sequencing data are compositional and therefore transformed for the variance analysis due to these data being relative values (Aitchison, 1982). Bioinformatic analyses were performed in R v4.2.1 and Rstudio (R Core Team, 2019) using the packages *vegan* (Oksanen et al., 2020) and *tidyverse* (Wickham et al., 2019) with the full code available on GitHub (see Data Availability Statement). Amplicon sequence variant (ASV) counts were standardized according to relative abundance by dividing an ASV's count by the total number of counts within a sample (McMurdie & Holmes, 2014). Alpha diversity was estimated using the Shannon-Weaver index by taking the mean over replicates. Statistical testing of the diversity between treatments was performed using one-way ANOVA and post hoc Tukey's HSD tests when correcting for multiple comparisons. Beta diversity was estimated using the Bray-Curtis dissimilarity index. A Redundancy Analyses (RDA) was performed to identify the relationship between the microbial community composition and environmental variables. The RDA models were assessed using permutation tests with generated biplots to visualize the influence of the explanatory variables.

2.4.8 | Summary of samples analysed

The main focus was on the start and end sampling, while for the mid sampling only microbiology and some basic geochemical variables were determined. TRS was not

determined for the surfaces as these were the outmost layers facing the atmosphere and thus, sulfide-minerals were not expected to be present. The SCE was carried out under normal laboratory conditions. It was thus not applied to the hypermonosulfidic sediment and the residues, as during the procedure there were risks of oxidation of the TRS-pool in these materials, which in turn, could have affected metal partitioning. Microbiology analysis was not performed on the residues.

2.5 | Use of medians for triplicates and samples analysed

Unless otherwise stated, the results of the triplicates of the control and each of the five treatments were reported as a median value.

3 | RESULTS AND DISCUSSION

3.1 | Character and representativeness of the hypermonosulfidic sediment

The sediment had high pH (7.8–8.0; $n = 3$), relatively high LOI values (5.3–5.8%; $n = 3$), consisted of approximately half of water by weight (48%; $n = 3$), and was black (Munsell N0). The total concentrations of the studied elements (S, Fe, Al, Ca, Mg, K and Na) are given in Table 1. The AVS concentrations (0.26–0.27; $n = 3$) were similar to those of the CRS concentrations (0.21%–0.28%), summing up to around half a percentage of TRS (median 0.52%, range 0.48%–0.54%). These physical and geochemical features are typical for this kind of fine-grained sediments occurring on the coastal plains in northern Europe (Åström & Björklund, 1997; Boman et al., 2008).

3.2 | Oxidation of the hypermonosulfidic sediment

In the aggregates of the control and all treatments by the end sampling, the AVS fraction had been almost completely lost (>97.5%) during the incubation (Table 2). In contrast, the CRS fraction had decreased to a smaller extent in the control (median 0.12%) and L10_{3.15 mm} (0.09%) and was preserved in the other treatments (medians 0.23%–0.27%). This pattern was correlated with the solid-phase Eh that by the end sampling had reached high values in the control (surface: 733 mV, aggregates: 697 mV), lower but still high values in L10_{3.15 mm} (surface: 533 mV, aggregates: 452 mV), but values of only 292–333 mV for surface and 265–314 mV for aggregates in

TABLE 1 Total concentrations of metals in the hypermonosulfidic sediment (bulk), as well as by the end sampling (25th month) in the residue, aggregates, and surface in the control and all five treatments.

Hypermonosulfidic sediment		Control	L10 _{3,15} mm	L40 _{3,15} mm	L10 _{2,5} μm	L40 _{2,5} μm	PL10 _{2,5} μm
Fe	Bulk, %	4.21 (4.02–4.36)					
	Residue, %	<i>n</i> ^a	4.37 (4.25–4.37)	4.29 (4.29–4.29)	4.36 (4.27–4.36)	4.8 (4.8–4.8)	4.27 (4.25–4.28)
	Aggregates, %	4.25 (4.24–4.46)	4.42 (4.28–4.48)	4.32 (4.24–4.35)	4.38 (4.19–4.6)	4.38 (4.14–4.45)	4.39 (4.32–4.53)
	Surface, %	4.94 (4.78–5.27)	4.14 (4.12–4.15)	4.14 (3.6–4.16)	4.19 (3.92–4.33)	4.4 (3.86–4.41)	4.29 (4.22–4.5)
	Leached Fe, mg	78 (15–160)	0.7 (0.7–1.0)	0.7 (0.4–1.0)	0.7 (0.6–0.8)	1.0 (0.6–1.5)	1.6 (1.1–2.9)
Al	Bulk, %	7.35 (7.1–7.51)					
	Residue, %	<i>n</i> ^a	7.21 (7.18–7.24)	7.09 (7.09–7.09)	7.08 (7.04–7.16)	7.22 (7.22–7.22)	7.32 (7.32–7.32)
	Aggregates, %	7.47 (7.15–7.56)	7.27 (6.84–7.88)	6.96 (6.84–7.41)	7.22 (7.19–7.4)	7.54 (7.1–7.56)	7.26 (7.26–7.53)
	Surface, %	6.84 (6.61–7.26)	6.83 (6.62–7.1)	6.66 (5.98–6.81)	6.9 (6.47–7.57)	6.79 (6.44–7.33)	6.8 (6.8–7.2)
	Leached Al, mg	460 (300–2100)	7 (3–7)	0.7 (0.4–1)	0.9 (0.7–1)	0.6 (0.5–0.8)	0.6 (0.5–0.8)
Mg	Bulk, %	1.38 (1.31–1.4)					
	Residue, %	<i>n</i> ^a	1.30 (1.24–1.31)	1.29 (1.29–1.29)	1.25 (1.25–1.28)	1.27 (1.27–1.27)	1.32 (1.32–1.32)
	Aggregates, %	1.28 (1.27–1.32)	1.3 (1.26–1.36)	1.27 (1.27–1.28)	1.28 (0.34–1.29)	1.33 (1.29–1.53)	1.36 (1.3–1.36)
	Surface, %	1.45 (1.39–1.58)	1.3 (1.28–1.37)	1.26 (1.25–1.45)	1.26 (1.25–1.43)	1.26 (1.25–1.4)	1.31 (1.28–1.33)
	Leached Mg, mg	2550 (2510–3850)	2100 (1700–2160)	1310 (1110–1410)	1570 (1150–1640)	1170 (1170–1230)	780 (590–1130)
K	Bulk, %	2.19 (1.43–2.33)					
	Residue, %	<i>n</i> ^a	1.96 (1.93–2.02)	2.12 (2.12–2.12)	2.54 (1.87–2.62)	2.6 (2.6–2.6)	2.25 (1.88–2.61)
	Aggregates, %	2.13 (1.79–2.67)	2.57 (2.21–2.87)	2.51 (2.45–2.52)	2.08 (1.82–2.57)	1.99 (1.82–2.92)	2.08 (1.92–2.73)
	Surface, %	2.49 (1.87–2.69)	1.95 (1.8–2.59)	2.18 (2.02–2.29)	2.46 (1.84–2.75)	2.17 (1.91–2.8)	2.46 (2.12–2.48)
	Leached K, mg	680 (570–940)	550 (500–570)	380 (350–430)	520 (350–530)	360 (340–390)	300 (200–400)
Na	Bulk, %	1.75 (1.64–1.8)					
	Residue, %	<i>n</i> ^a	1.62 (1.61–1.66)	1.58 (1.58–1.58)	1.67 (1.67–1.73)	1.56 (1.56–1.56)	1.61 (1.59–1.63)
	Aggregates, %	1.66 (1.64–1.7)	1.7 (1.64–1.75)	1.59 (1.59–1.62)	1.73 (1.7–2.07)	1.59 (1.57–1.72)	1.67 (1.63–1.71)
	Surface, %	1.61 (1.53–1.61)	1.61 (1.6–1.68)	1.51 (1.46–1.64)	1.62 (1.6–1.72)	1.5 (1.49–1.73)	1.63 (1.58–1.67)
	Leached Na, mg	3720 (2720–4120)	3950 (3700–4280)	3400 (3180–3510)	4650 (3080–4750)	3400 (3180–3570)	3000 (1910–3660)
Ca	Bulk, %	1.33 (1.25–1.38)					
	Residue, %	<i>n</i> ^a	1.84 (1.77–1.97)	3.59 (3.59–3.59)	1.99 (1.91–1.99)	3.42 (3.42–3.42)	1.91 (1.9–1.91)
	Aggregates, %	1.22 (1.21–1.23)	1.63 (1.57–1.68)	3.43 (3.27–3.84)	1.69 (1.55–1.71)	3.24 (2.98–3.29)	1.64 (1.6–1.75)
	Surface, %	1.8 (1.6–1.83)	2.46 (2.33–2.64)	4.45 (3.49–5.55)	2.61 (2.27–2.69)	4.12 (3.91–4.35)	2.4 (1.89–2.54)
	Leached Ca, mg	1660 (1500–2170)	6850 (5510–6930)	4450 (3840–4500)	5270 (3650–5430)	3740 (3280–4090)	2300 (1790–3540)

Note: The total mass (mg) of metals cumulatively leached via the drainage water from the incubation cells are indicated. The data is presented as medians (min and max) in %.

^aNo residue.

TABLE 2 Concentrations of total sulfur, AVS, CRS and other S-species in the hypermonosulfidic sediment (bulk), as well as by the end sampling (25th month) in the residues and aggregates (and additionally for total S in the surface) in the control and all five treatments.

Hypermonosulfidic sediment		Control	L10 _{3,15} mm	L40 _{3,15} mm	L10 _{2,5} μm	L40 _{2,5} μm	PL10 _{2,5} μm
Total S	Bulk	0.78 (0.66–0.92)					
	Residue	<i>n</i> ^a	0.78 (0.78–0.79)	0.72 (0.72–0.72)	0.69 (0.69–0.69)	0.72 (0.72–0.72)	0.75 (0.70–0.79)
	Aggregates	0.37 (0.30–0.42)	0.39 (0.36–0.46)	0.42 (0.29–0.45)	0.42 (0.42–0.54)	0.41 (0.30–0.46)	0.41 (0.38–0.59)
	Surface	1.58 (1.08–2.10)	1.51 (1.07–1.59)	1.57 (1.32–2.49)	1.20 (0.97–1.39)	1.23 (1.16–1.50)	0.65 (0.44–1.33)
AVS	Bulk	0.27 (0.26–0.27)					
	Residue	<i>n</i> ^a	0.25 (0.24–0.27)	0.26 (0.26–0.26)	0.21 (0.21–0.21)	0.21 (0.2–0.23)	0.31 (0.29–0.31)
	Aggregates	0.002 (0.001–0.005)	0.004 (0.002–0.006)	0.006 (0.001–0.01)	0.005 (0.002–0.006)	0.004 (0.001–0.01)	0.006 (0.003–0.14)
CRS	Bulk	0.25 (0.21–0.28)					
	Residue	<i>n</i> ^a	0.36 (0.35–0.37)	0.32 (0.31–0.33)	0.29 (0.29–0.3)	0.28 (0.28–0.28)	0.28 (0.25–0.33)
	Aggregates	0.12 (0.03–0.13)	0.1 (0.08–0.2)	0.25 (0.18–0.28)	0.27 (0.26–0.3)	0.27 (0.16–0.3)	0.23 (0.22–0.43)
Other S-species	Bulk	0.26 (0.19–0.37)					
	Residue	<i>n</i> ^a	0.17 (0.17–0.17)	0.14 (0.14–0.14)	0.18 (0.18–0.18)	0.22 (0.22–0.22)	0.15 (0.14–0.17)
	Aggregates	0.27 (0.24–0.3)	0.27 (0.19–0.36)	0.17 (0.11–0.19)	0.16 (0.13–0.26)	0.14 (0.13–0.16)	0.17 (0.15–0.17)
Leached sulfur, g		8.51 (7.55–11.89)	10.49 (8.66–10.65)	6.43 (5.85–6.86)	8.12 (5.74–8.26)	5.54 (5.19–6.09)	3.39 (2.65–5.0)

Note: The total mass of sulfate, reported as S, cumulatively leached via the drainage waters are also presented. Other S-species were calculated by difference: Total S—the sulfide fractions. The data is presented as medians (min and max) in %.

^aNo residue.

the other treatments (Figure 2b), representing moderately reduced soil conditions (Kaurichev & Shishova, 1967). The Eh in the drainage waters showed overall higher values, but similar features as for the solid phase (Figures 1b and 2b). Furthermore, residues did not exist for the control and occurred in the treatments in estimated decreasing proportions from $PL10_{2.5\ \mu\text{m}}$ (70%) > $L10_{2.5\ \mu\text{m}}$ (30%) > $L40_{2.5\ \mu\text{m}}$ (20%) = $L10_{3.15\ \text{mm}}$ (20%) > $L40_{3.15\ \text{mm}}$ (0%). The residues had similar physical appearance (massive), colour, and concentrations of total S, AVS and CRS as the hypermonosulfidic sediment (Table 2) and thus, had remained unoxidized. Taken together, these features showed that the oxidation became subdued when limestone was added, in particular the fine-grained variant, but as basically the entire AVS pool was oxidized in the aggregates (and in the control and $L10_{3.15\ \text{mm}}$ additionally a large part of the CRS pool), proton production had been extensive.

3.3 | pH response to oxidation and treatments

The control drainage-water pH dropped rapidly (Figure 1a) and ended around pH 3.5 both in the aqueous and solid phases (Figures 1a and 2a), which are typical values for this kind of sediment when oxidized under field conditions (Johnson et al., 2022; Nyman et al., 2023; Österholm & Åström, 2002). In $L10_{3.15\ \text{mm}}$, the pH in the drainage water dropped stepwise and ended at 4.3 (Figure 1a), and in the solid phase ended at similar (slightly higher) values (Figure 2a). Consequently, addition of the coarse-grained limestone in amounts corresponding to a theoretical 100% neutralization demand of the potential acidity of all TRS caused the pH not to drop to the typical sub-4.0 level but was unable to prevent a drop to sub-5.0. In contrast, for $L10_{2.5\ \mu\text{m}}$ the pH of the solid phase was maintained around 8.0 (Figure 2a) and for the drainage water remained near neutral (Figure 1a). There was thus a clear effect of the limestone grain size, with the smaller size hindering a pH drop from near neutral. Possible explanations and underlying mechanisms are discussed in Section 3.7. Adding peat to the fine-grained variant resulted in a moderate decrease in pH in the drainage water towards the end (Figure 1a). For $L40_{3.15\ \text{mm}}$ and $L40_{2.5\ \mu\text{m}}$ pH remained high throughout.

3.4 | Leaching of chloride: Mobilization of trapped sea salts

The Cl^- concentrations decreased over time in a similar manner for the control and the treatments, starting with high values in the beginning (508–768 mg/L) and finishing

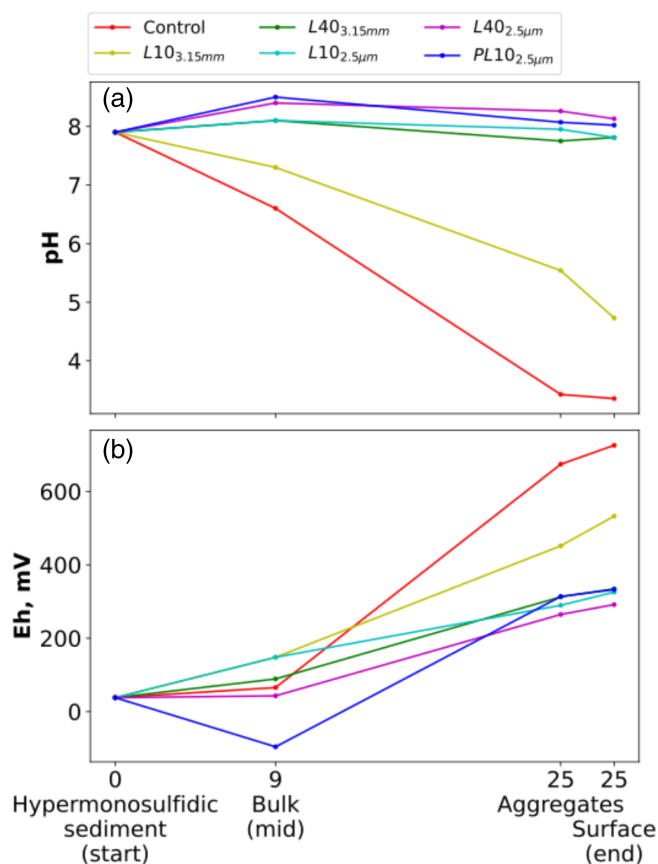


FIGURE 2 Median pH (a) and median Eh (b) of the hypermonosulfidic sediment (start), a bulk sample of the material after 9 months (mid sampling), and in the aggregates and surface after 25 months (end sampling).

with low values (≤ 10 mg/L) towards the end of the experiment (Figure 11). The cumulative amount of Cl^- leached was highest for $L10_{2.5\ \mu\text{m}}$ (3.2 g) and for the others smaller and within a rather narrow range ($PL10_{2.5\ \mu\text{m}}$ 2.0 g, $L40_{2.5\ \mu\text{m}}$ 2.2 g, control 2.2 g, $L40_{3.15\ \text{mm}}$ 2.3 and $L10_{3.15\ \text{mm}}$ 2.5). These values corresponded to a range of 530–830 mg/L of initial Cl^- concentrations in the pore water with an initial volume of 3.84 L (48% of the weight of the 8000 g wet sediment). The similarity in values, regardless of residue levels, indicated that Cl^- had also been leached from the residues. Consequently, the residues had not been exposed to oxygen as its sulfide mineralogy was unaltered but was susceptible to anion diffusion.

3.5 | Leaching of Na, K, Mg and Si: Sum effects of various geochemical reactions

As for Cl^- , the dissolved concentrations of Na decreased during the incubation in a similar manner for the control and all treatments, starting with high values at the beginning (370–480 mg/L) and finishing with low values towards

the end (10–38 mg/L) of the experiment (Figure 1i). In the first measurement, the Na to Cl^- ratio was typically 0.6–0.7 (w/w) and thus similar to that in seawater, indicating leaching of pore-water (seawater derived) Na. Thereafter, the ratio continuously increased reaching values >2.0 after 7 months. The excess Na was not explained by weathering of Na-bearing silicates, as this certainly would have been reflected in higher values for the control that was acidic than for the near-neutral limestone treatments, which was not the case. Instead, it was likely related to the exchange of Na^+ on mineral surfaces with protons and Al^{3+} in the control and Ca^{2+} in the limestone-treated sediments. In contrast, the leaching of Mg, K, and Si was lower in L40_{3.15 mm}, L40_{2.5 μm}, L10_{2.5 μm} and PL10_{2.5 μm} than in L10_{3.15 mm} in which it was lower than in the control (Figure 1h,j,k). This suggested that the pH increase caused by the limestone treatments slowed down the rate of weathering of silicates such as mica, amphibole and K-feldspar that occur in the sediments (Åström & Björklund, 1997).

3.6 | Fate of Fe, S, Ca and Al

For the control, which was oxidized throughout (no residues), the amounts of Fe leached via the drainage water represented only a very minor part (0.043%) of the total Fe content in the sediment. For the treatments, even less Fe was leached, corresponding to only around 1.0% of that leached from the control (Table 1). Hence, the vast majority of the Fe that was released during the oxidation of sulfides and weathering of silicates (mica and amphibole) remained in the sediment. In the control, a characteristic feature of the total Fe solid-phase data was the enrichment in the surface (Table 1). This showed that Fe had migrated from aggregates to surfaces in the acidic environment, most likely in the form of Fe^{2+} and subsequently, was precipitated on the surfaces as typically seen also under field conditions in acid sulfate soils developed on this sediment type (Yu, Luong, et al., 2024). The XAS analyses suggested that the precipitation was in the form of schwertmannite (mineral proportions obtained by linear combination fitting: hornblende 0.34%, illite 0.32%, schwertmannite 0.31%), in line with this mineral making up a significant part of the secondary Fe(III) pool on crack surfaces of acid sulfate soils both in the boreal zone (Yu et al., 2023) and elsewhere (Collins et al., 2010; Fitzpatrick et al., 2017; Shahabi-Ghahfarokhi et al., 2022; Vithana et al., 2015). In contrast, in the treatments, Fe was not enriched in the surface (Table 1) but was more extractable with HXL than in the control, that is, 0.75%–0.81% as compared with 0.74% for the surface and 0.71%–0.83% as compared with 0.59% for the aggregates (Table 3). These HXL-extractable features suggested that

first, schwertmannite in the surface of the control was only partially extracted with this reagent and thus consisted (at least partly) of a more crystalline variant (a relatively high Fe to S ratio) that requires a stronger (i.e., 1 M) HXL extraction than was used (Chen et al., 2022). Secondly, formation of ferrihydrite in the treatments, a mineral that dissolves easily with the HXL extractant, and is frequently seen in soils developed on this kind of sediment (Yu, Luong, et al., 2024). This is further in line with the typical stability fields of these minerals with schwertmannite forming under acidic sulfate-rich conditions and ferrihydrite under near-neutral conditions (Schoepfer & Burton, 2021; Zachara et al., 2002). Furthermore, in the treatments as in the control, relatively large amounts of Fe were extractable with NaOAc, ranging from 0.16% to 0.24% (Table 3). Iron thus existed in relatively large amounts also in an easily extractable form, which may be susceptible to mobilization under changing conditions. This may trigger abundant Fe leaching, which is frequently seen from acid sulfate soils both in the hemiboreal zone (Shahabi-Ghahfarokhi et al., 2022) and elsewhere (Enio et al., 2020; Sukitprapanon et al., 2018).

In contrast with Fe, sulfate was abundant in the drainage water both from the control and treatments (Figure 1d), with cumulative amounts (recalculated to S) leached decreasing in the order L10_{3.15 mm} (10.5 g) $>$ control (8.5) $>$ L10_{2.5 μm} (8.1) $>$ L40_{3.15 mm} (6.4) $>$ L40_{2.5 μm} (6.1) and $>$ PL10_{2.5 μm} (3.4). When calculating the S content initially contained in the aggregates plus surfaces, that is excluding the residues where there had been no oxidation of sulfide (and thus no leaching of sulfate), the percentage of S lost via the drainage water was overall relatively low but higher for the low-limestone treatments (L10_{3.15 mm} 40%; L10_{2.5 μm} 36%, PL10_{2.5 μm} 35%) than for the high-limestone treatments (L40_{2.5 μm} 21%, L40_{3.15 mm} 20%) and the control (26%). Although pyrite remained to various extents in the aggregates, these relatively low percentages showed that part of the formed sulfate had been retained in the sediment, in particular when limestone was added in excess. The explanation was found in the solid-phase data showing substantial enrichment of total S in the surface both in the control and treatments (Table 2). Consequently, in the aggregates which had depleted S concentrations (Table 2), following AVS oxidation (and for the control and L10_{3.15 mm} also pyrite oxidation), sulfate had migrated and was subsequently partly retained in the surface.

The sulfate retention in the surface was due to formation of various sulfate minerals. In the control, the Fe oxyhydroxysulfate mineral schwertmannite occurred. This was consistent with this mineral forming under the acidic conditions that rapidly developed in the control

TABLE 3 Sequential chemical extraction (SCE) of metals for the surface and aggregate samples applying successively sodium acetate (NaOAc), tetrasodium pyrophosphate (TSPP), and 0.25 M hydroxylamine hydrochloride (HXL).

	Surface				Aggregates				
	NaOAc	TSPP	HXL	Residual	NaOAc	TSPP	HXL	Residual	
Fe	Control	0.24 (0.24–0.24)	0.19 (0.19–0.19)	0.74 (0.66–0.75)	3.60 (3.76–4.18)	0.17 (0.17–0.18)	0.13 (0.12–0.13)	0.59 (0.58–0.59)	3.38 (3.34–3.50)
	L10 _{3,15} mm	0.24 (0.19–0.27)	0.16 (0.16–0.19)	0.75 (0.67–0.81)	2.98 (2.94–3.05)	0.17 (0.12–0.19)	0.17 (0.16–0.19)	0.71 (0.70–0.83)	3.28 (3.23–3.42)
	L40 _{3,15} mm	0.16 (0.14–0.17)	0.12 (0.09–0.17)	0.79 (0.68–0.80)	3.03 (2.66–3.07)	0.20 (0.19–0.20)	0.12 (0.10–0.14)	0.83 (0.73–0.83)	3.17 (3.12–3.26)
	L10 _{2,5} μm	0.20 (0.13–0.21)	0.14 (0.14–0.19)	0.80 (0.77–0.84)	3.10 (2.77–3.14)	0.19 (0.18–0.24)	0.17 (0.14–0.18)	0.81 (0.77–0.81)	3.04 (2.94–3.16)
	L40 _{2,5} μm	0.17 (0.16–0.20)	0.13 (0.09–0.17)	0.81 (0.70–0.85)	2.90 (2.86–3.26)	0.19 (0.18–0.21)	0.14 (0.12–0.16)	0.77 (0.71–0.77)	3.30 (3.05–3.38)
	PL10 _{2,5} μm	0.23 (0.16–0.23)	0.22 (0.14–0.26)	0.78 (0.75–0.78)	3.21 (2.99–3.26)	0.19 (0.12–0.24)	0.19 (0.16–0.19)	0.79 (0.75–0.82)	3.24 (3.20–3.33)
Al	Control	0.11 (0.10–0.29)	0.07 (0.04–0.08)	0.35 (0.26–0.36)	6.31 (6.31–6.89)	0.05 (0.05–0.06)	0.46 (0.32–0.51)	0.31 (0.30–0.33)	7.03 (6.98–7.14)
	L10 _{3,15} mm	0.03 (0.02–0.03)	0.03 (0.03–0.03)	0.30 (0.27–0.32)	6.28 (6.25–6.73)	0.03 (0.02–0.03)	0.03 (0.03–0.03)	0.32 (0.29–0.35)	6.86 (6.78–7.75)
	L40 _{3,15} mm	0.02 (0.01–0.02)	0.02 (0.01–0.02)	0.31 (0.27–0.31)	6.31 (5.68–6.49)	0.03 (0.02–0.03)	0.02 (0.01–0.02)	0.32 (0.29–0.33)	6.48 (6.47–6.63)
	L10 _{2,5} μm	0.02 (0.02–0.03)	0.02 (0.02–0.03)	0.32 (0.32–0.34)	6.54 (6.45–7.18)	0.03 (0.02–0.03)	0.03 (0.02–0.02)	0.32 (0.31–0.35)	7.02 (6.82–7.04)
	L40 _{2,5} μm	0.02 (0.02–0.02)	0.02 (0.01–0.02)	0.31 (0.29–0.32)	6.12 (6.12–6.98)	0.02 (0.02–0.03)	0.02 (0.02–0.02)	0.32 (0.30–0.33)	6.86 (6.74–7.21)
	PL10 _{2,5} μm	0.02 (0.02–0.02)	0.02 (0.02–0.03)	0.31 (0.31–0.33)	6.45 (6.43–6.83)	0.02 (0.02–0.02)	0.02 (0.02–0.03)	0.32 (0.31–0.36)	7.13 (6.89–7.19)
Mg	Control	0.31 (0.15–0.48)	0.01 (0.01–0.02)	0.13 (0.11–0.13)	1.12 (0.83–1.12)	0.01 (0–0.01)	0.05 (0.04–0.06)	0.14 (0.13–0.14)	1.10 (1.09–1.12)
	L10 _{3,15} mm	0.26 (0.10–0.37)	0.01 (0.01–0.01)	0.14 (0.13–0.15)	0.87 (0.86–1.04)	0.07 (0.05–0.10)	0.01 (0.01–0.01)	0.15 (0.13–0.16)	1.04 (1.03–1.17)
	L40 _{3,15} mm	0.23 (0.13–0.25)	0.01 (0.01–0.01)	0.16 (0.14–0.16)	0.96 (0.88–1.03)	0.09 (0.09–0.11)	0.01 (0.01–0.01)	0.16 (0.14–0.16)	1.01 (1.00–1.04)
	L10 _{2,5} μm	0.12 (0.09–0.18)	0.01 (0.01–0.01)	0.16 (0.15–0.16)	1.00 (0.98–1.08)	0.05 (0.05–0.10)	0.01 (0.01–0.01)	0.15 (0.15–0.16)	1.07 (1.06–1.08)
	L40 _{2,5} μm	0.12 (0.09–0.14)	0.01 (0.01–0.01)	0.15 (0.15–0.16)	1.00 (0.99–1.10)	0.08 (0.07–0.11)	0.01 (0.01–0.01)	0.15 (0.14–0.15)	1.10 (1.05–1.28)
	PL10 _{2,5} μm	0.18 (0.12–0.23)	0.01 (0.01–0.01)	0.15 (0.15–0.15)	0.94 (0.94–1.04)	0.08 (0.06–0.09)	0.01 (0.01–0.01)	0.16 (0.15–0.16)	1.11 (1.05–1.15)
K	Control	0.10 (0.07–0.32)	0.04 (0.03–0.05)	0.11 (0.06–0.11)	2.24 (1.40–2.54)	0.06 (0.06–0.06)	0.04 (0.03–0.05)	0.06 (0.06–0.07)	1.97 (1.62–2.52)
	L10 _{3,15} mm	0.17 (0.10–0.17)	0.03 (0.03–0.04)	0.05 (0.05–0.06)	1.70 (1.54–2.41)	0.15 (0.10–0.31)	0.04 (0.04–0.05)	0.06 (0.05–0.06)	2.32 (1.80–2.69)
	L40 _{3,15} mm	0.12 (0.12–0.28)	0.04 (0.03–0.04)	0.05 (0.05–0.05)	1.97 (1.65–2.10)	0.15 (0.15–0.16)	0.03 (0.03–0.04)	0.05 (0.05–0.05)	2.27 (2.22–2.28)
	L10 _{2,5} μm	0.18 (0.10–0.33)	0.03 (0.03–0.05)	0.05 (0.05–0.06)	2.28 (1.41–2.49)	0.10 (0.10–0.17)	0.03 (0.03–0.04)	0.05 (0.05–0.06)	2.25 (1.90–2.38)
	L40 _{2,5} μm	0.11 (0.10–0.22)	0.04 (0.02–0.04)	0.05 (0.05–0.05)	1.99 (1.60–2.60)	0.16 (0.11–0.29)	0.04 (0.04–0.04)	0.05 (0.05–0.05)	1.80 (1.45–2.67)
	PL10 _{2,5} μm	0.16 (0.16–0.30)	0.04 (0.04–0.04)	0.05 (0.05–0.05)	2.22 (1.73–2.22)	0.29 (0.10–0.30)	0.04 (0.04–0.05)	0.06 (0.05–0.06)	1.67 (1.52–2.54)
Ca	Control	0.64 (0.56–0.71)	0.30 (0.30–0.30)	0.04 (0.04–0.08)	1.18 (0.79–1.18)	0.05 (0.04–0.05)	0.30 (0.30–0.30)	0.08 (0.08–0.08)	1.07 (1.07–1.08)
	L10 _{3,15} mm	2.20 (1.26–2.35)	0.03 (0.03–0.06)	0.10 (0.07–0.10)	0.16 (0.13–0.95)	0.64 (0.36–0.65)	0.30 (0.30–0.30)	0.10 (0.08–0.10)	0.92 (0.86–1.11)
	L40 _{3,15} mm	4.57 (2.66–5.25)	0.10 (0.08–0.10)	0.09 (0.07–0.10)	0.15 (0–0.63)	3.47 (3.05–4.01)	0.08 (0.07–0.12)	0.10 (0.08–0.11)	0 (0–0.06)
	L10 _{2,5} μm	1.76 (1.70–2.29)	0.06 (0.06–0.07)	0.09 (0.08–0.10)	0.43 (0.25–0.68)	0.56 (0.34–0.70)	0.03 (0.03–0.03)	0.09 (0.09–0.09)	1.03 (0.88–1.10)
	L40 _{2,5} μm	3.34 (2.68–3.38)	0.09 (0.06–0.11)	0.09 (0.08–0.10)	0.76 (0.42–1.27)	2.53 (2.43–2.83)	0.08 (0.07–0.08)	0.09 (0.09–0.10)	0.29 (0.28–0.65)
	PL10 _{2,5} μm	1.40 (0.92–1.40)	0.06 (0.03–0.08)	0.08 (0.04–0.10)	0.53 (0.46–0.86)	0.54 (0.44–0.80)	0.03 (0.03–0.05)	0.09 (0.08–0.10)	0.94 (0.81–1.09)

Note: Residuals were calculated by difference: Total concentration—the three SCE steps. The data is presented as median (min and max) in %.

cells (Fitzpatrick et al., 2017; Schoepfer & Burton, 2021). Furthermore, both gypsum and sanderite were identified by XRD in precipitates picked from the surfaces (SI4). This showed that sulfate was not only leached and trapped by formation of oxhydroxysulfates, but also was forming salts with both Ca and Mg. The source of these metals were certainly Mg- and Ca-bearing aluminosilicates that exist in these sediments (Åström & Björklund, 1997) and would have been susceptible to weathering under the acidic conditions (Ezzaim et al., 1999). For L10_{3.15 mm}, which became only weakly acidic and had no Fe enrichment in the surface (Table 1), formation of schwertmannite was unlikely, at least in significant amounts. Instead, the precipitates on the surface had, relative to the control, clearly higher atomic percentages of Mg and S, and lower atomic percentages of Ca (Table SI3). This was consistent with first, the XRD identification of Mg sulfates (caminite and sanderite) but also gypsum; second, the SEM images showing an abundance of Mg sulfates with pronounced elongated crystals and good cleavage but very little gypsum flakes (Figure SI1, Table SI3); and third, abundant leaching of Ca (highest of all treatments) but relatively low leaching of Mg (Figure 1h). These features may be due to Mg ions affecting both the nucleation and growth of gypsum crystals. By substituting for Ca in the gypsum lattice, Mg alters the crystal structure and increases gypsum solubility (Ben Ahmed et al., 2014). Hence, Mg-sulfate precipitation was favoured in these cells. In contrast, for L10_{2.5 μm} that had equally much limestone added as L10_{3.15 mm}, the precipitates picked from the surface were different. The SEM-EDS analyses showed that the Ca concentrations were strongly increased, whereas those of Mg strongly decreased, consistent with the XRD analyses identifying only gypsum (Figure SI2) and the SEM images showing distinct gypsum plates (Figure SI1). These data indicated that the near-neutral pH conditions and addition of fine-grained limestone favoured Ca-sulfate over Mg-sulfate precipitation (Uhlmann et al., 2004). In the treatment where peat was added (PL10_{2.5 μm}), there was again a change in the precipitates that looked like a loose, earthy mass with rare needle-shaped crystals (Figure SI1) and that had relatively low concentrations of Ca, Mg and S. Instead, the C concentrations were strongly increased (34%) indicating an abundance of organic compounds, in line with the peat added to this treatment. The precipitates from this treatment were further separated into 'grey' and 'white' for XRD analysis due to a noticeable colour difference between the particles. The 'grey' fraction included three different hydrated Mg sulfates: epsomite, hexahydrate and sanderite, while the 'white' fraction contained the less hydrated Mg sulfate kieserite plus gypsum. The small amount of gypsum in these

precipitates can be attributed to the influence of the organic compounds, as fulvic acid acts as an inhibitor in the gypsum precipitation process affecting both the morphology and size of the crystals (Xu et al., 2019). This leads to the formation of thinner and shorter gypsum crystals as compared with those formed in L10_{2.5 μm} (Figure SI1). Additionally, at near-neutral pH, which this treatment had, the electrostatic interactions between fulvic acids and gypsum intensify due to their opposite charges that further inhibit gypsum precipitation (Xu et al., 2019). Taken together, these data and features indicated a high diversity in the formation of sulfate salts, with no systematic difference between the treatments and control. For the high-limestone treatments there was no mineralogical data, but their low percentages of sulfate leaching indicated that when limestone was added in excess, formation of sulfate salts was even more favourable.

The total Ca concentration in the hypermonosulfidic sediment was 1.33% (Table 1). In the residues of the treatments the concentrations were increased (Table 1) to an extent that corresponded to the added Ca as limestone. This suggested that the limestone particles were preserved in the residues, in line with the unaltered sulfide mineralogy and thus, no proton production within this part of the sediment. The Ca concentrations were decreased in the aggregates and elevated in the surface both in the treatments and control, in a manner similar to S (Table 1). For the treatments, this was explained by carbonate dissolution by protons from sulfide oxidation in the aggregates (such dissolution certainly occurred also in the surface) with concomitant migration of Ca²⁺ that was partly retained in the surface. As the Ca in the surface was dissolved by NaOAc in high levels (Table 3), the retention occurred via formation of easily dissolved phases, in line with the occurrence of gypsum in picked precipitates (SI4). Like S, Ca was also abundant in the drainage waters (Figure 1e), with the cumulative leaching being higher for L10_{3.15 mm} and L10_{2.5 μm} (6.8 and 5.3 g, respectively) than L40_{3.15 mm} and L40_{2.5 μm} (4.4 and 3.7, respectively), and lowest for PL10_{2.5 μm} (2.3 g). When comparing with the limestone content initially contained in the aggregates plus surfaces (excluding the residues where the limestone was intact), the percentage of Ca lost via the drainage water corresponded to 36%, 32% and 31% for L10_{3.15 mm}, PL10_{2.5 μm} and L10_{2.5 μm}, respectively, and 5% for both L40_{3.15 mm} and L40_{2.5 μm}. These values were upper limits as it was likely that Ca was also mobilized from inherent phases, which at least under the acidic conditions in the control was quite large (1.7 g). The relatively low percentages also for the low-carbonate treatments was in line with unreleased acidity (and thus unaffected carbonate) as all TRS was not

dissolved plus the secondary Ca enrichment in the surface. The highest leaching for L10_{3.15 mm} correlated with this treatment having a higher proportion of oxidized TRS than the other treatments (Table 2).

The cumulative leaching of Al via the drainage water from the treatments (0.6–7 mg) was only a fraction of that leached from the control (460 mg; Table 1; Figure 1g), showing the well-established large effect of pH on Al solubility (Cappuyns & Swennen, 2008; Goodman et al., 2023). Furthermore, Al extracted with NaOAc and TSPP were in the treatments decreased as compared with the control (Table 3). This showed that the pH neutralization by the limestone efficiently prevented not only Al leaching via the drainage water, but also build-up of a labile Al pool in the solid phase.

3.7 | Differences in the effects of various limestone grain sizes

As presented above, when applied in amounts corresponding to a theoretical 100% neutralization of all potential TRS-derived acidity, the fine-grained limestone variant prevented a pH drop from near-neutral while with the coarse-grained variant pH dropped to <5.0. The most obvious difference between these treatments was that the coarse-grained particles have a much smaller total surface area and thus, less likely to react with protons produced by sulfide oxidation (Zhu et al., 2023), and are more likely to become, to a large extent, covered by secondary minerals that can cause inactivation of the limestone grains (Caldeira et al., 2003). Such inactivation very likely occurred in particular via Fe coating, as there was minimal leaching but high HXL-extractability of Fe (Table 3) suggesting abundant formation of ferrihydrite that can easily cause this coating. However, as compared with the coarse-grained variant, the fine-grained variant resulted in preservation of pyrite and maintained a lower Eh value both in the solid phase (aggregates, surfaces) and drainage waters (Figures 1b and 2b). Consequently, the effect of the fine-grained variant may also have been to slow down the oxidation. As shown in early work (Warren, 1956), the addition of calcium carbonate to a pyrite suspension drastically reduces the rate of pyrite oxidation. Furthermore, Caldeira et al. (2003) show that the oxide layer formed on pyrite particles in a carbonate-rich environment is mainly ferrihydrite. Therefore, a possible explanation for the preservation of pyrite at high pH values in the L10_{2.5 μm} could be a restricted contact between the sulfide and oxygen by a layer of ferrihydrite. Ferrihydrite is not stable at lower pH values, which could explain why the pyrite in

L10_{3.15 mm} was only partially preserved. Whichever mechanism dominated, the effect of the fine-grained variant was positive as it either prevents a drop in pH in the long term or prolongs the acidity formation, thus minimizing the risk of acute acid shocks.

3.8 | The effects of peat

In the treatment where peat was added to the fine-grained limestone (10 kg/m³), the pH of the water remained close to neutral until month 26, after which it began to decline and reached a value of 5.1 at month 30 (Figure 1a). This pH drop was likely linked to the decomposition of peat. This process leads to the formation of organic acids that contribute to acidification (Saarinen et al., 2013) and is likely to form coatings on the limestone grains thus reducing their neutralizing capacity (Chan & Heenan, 1999; Shoty, 1988). Furthermore, the cumulative leaching of Fe via the drainage water was higher from the peat treatment than the other treatments (Table 1) possibly due to formation of labile iron-organic complexes (Yu et al., 2023). However, this treatment stood out as having by far the highest estimated proportion of residues (70% as compared with 0%–30% for the other treatments and 0% for the control), which showed that the peat significantly slowed down the movement of the oxidation front. This may have been due to the consumption of oxygen by organic matter decomposition, thus preventing oxidation of AVS deep into the sediment.

3.9 | Microbiology

3.9.1 | 16S rRNA gene sequencing data

The Illumina 16S rRNA gene amplicon sequencing of the 57 samples gave a total of 9,113,104 Kreads that averaged 159,879 ± 48,754 Kreads per sample (minimum of 61,837 and maximum 306,826; Table S15) of which 16.9% were filtered out during the quality control steps. Sufficient sequencing depth to identify the majority of microbial taxa was supported by the asymptotic curves of the rarefaction analysis (Figure S13).

3.9.2 | 16S rRNA gene sequence-based community diversity

ANOVA and Tukey's post hoc (Figure S14) testing for Shannon's alpha diversity showed no significant differences between treatments, sampling period, or material sampled. However, the ANOVA of richness showed

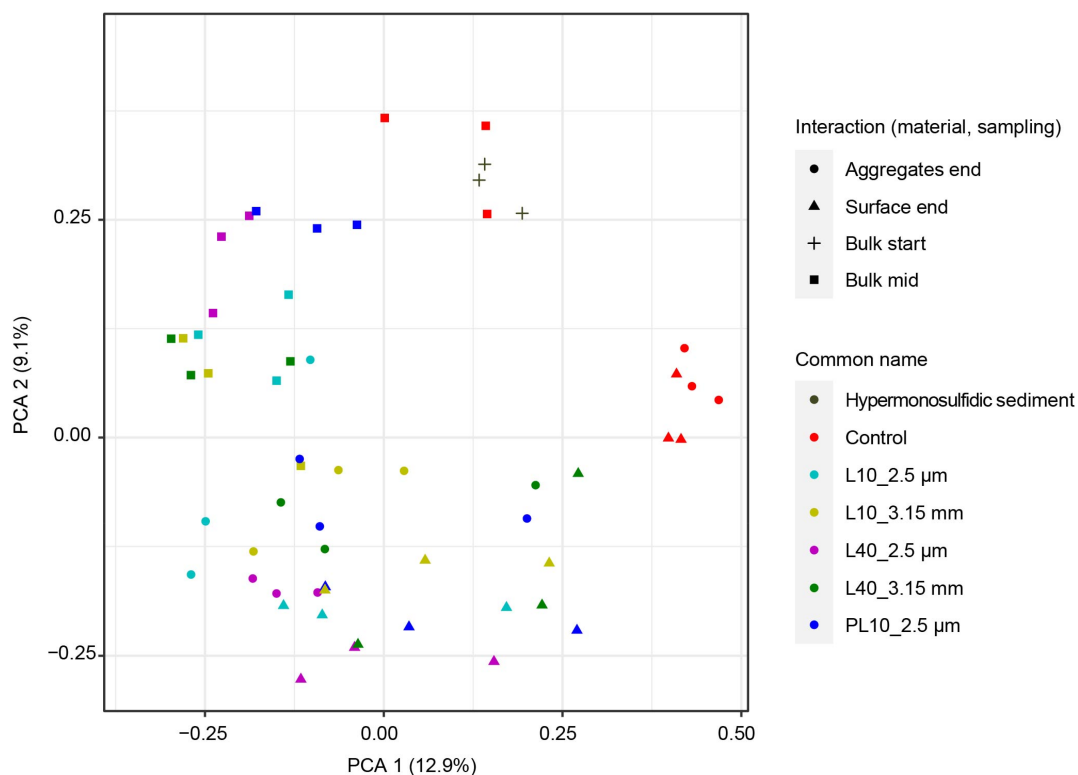


FIGURE 3 Unconstrained principal components analysis (PCA) showing Bray–Curtis dissimilarity of the 16S rRNA gene amplicon-based microbial communities from the hypermonosulfidic sediment, the control, and the five treatment as well as the three sampling periods.

significance when comparing sampling periods ($p \leq 0.01$) and Tukey's post hoc testing showed significance for the pairwise comparisons of control—end—aggregates compared with L10_{3.15 mm}—mid—bulk ($p = 0.01$) and control—end—aggregates compared with PL10_{2.5 μm}—mid—bulk ($p = 0.01$). Finally, the ANOVA and Tukey's post hoc tests of Pielou's evenness were insignificant.

The principal component analysis (PCA) of the microbial sequences Bray–Curtis dissimilarity is presented in Figure 3 with 22% of the total variability explained by the two axes. Along the first axis, the control end samples (aggregates and surface) were clearly separated from the others, and along the second axis two groupings were separated according to the sampling period where one group consisted of the hypermonosulfidic sediment and mid samples, and the second group of the end samples (surface and aggregate). A redundancy analysis (RDA) incorporating physiochemical variables showed similar features but only explained 6.2% of the microbial sequence data variability (Figure 4). Along the first axis there was a separation of the hypermonosulfidic sediment plus mid samples correlating with lower Eh (redox) and dry weights for these than the end samples. Along the second axis there was a general separation of the control from the L10_{3.5 mm} and the rest correlating with the variability in pH and Eh.

Despite insignificant differences in the Shannon's diversity and Pielou's evenness, the PCA and RDA suggested a deviation in the microbial communities as a result of the liming treatments that was supported by the significant differences in richness. In addition, there were differences in the taxa present as a result of the treatments.

3.9.3 | Microbial community composition

The 16S rRNA gene amplicon sequences of the top 20 most relative abundant taxa across all samples at the phylum level (Figure S15) were dominated by ASVs aligning to Proteobacteria (mean relative abundances across all treatments 31.8%), Desulfobacterota (5.0%), Bacteriota (3.4%), Chloroflexota (3.0%), Actinobacteriota (2.2%) and Acidobacteriota (2.0%).

The hypermonosulfidic sediment (pH 7.9) had a high relative abundance of the potential sulfur and sulfate reducing (amalgamated as SRB) 34–128 family (29.1% mean relative abundance; Figure 5) from the phylum Caldatribacteriota (Dong et al., 2022), which is associated with deep sea cold seep sediments (Parks et al., 2017). This is in line with the sediment characteristics, including presence of metastable iron sulfides and pyrite, a low Eh, a marine source, and formed in a low-temperature

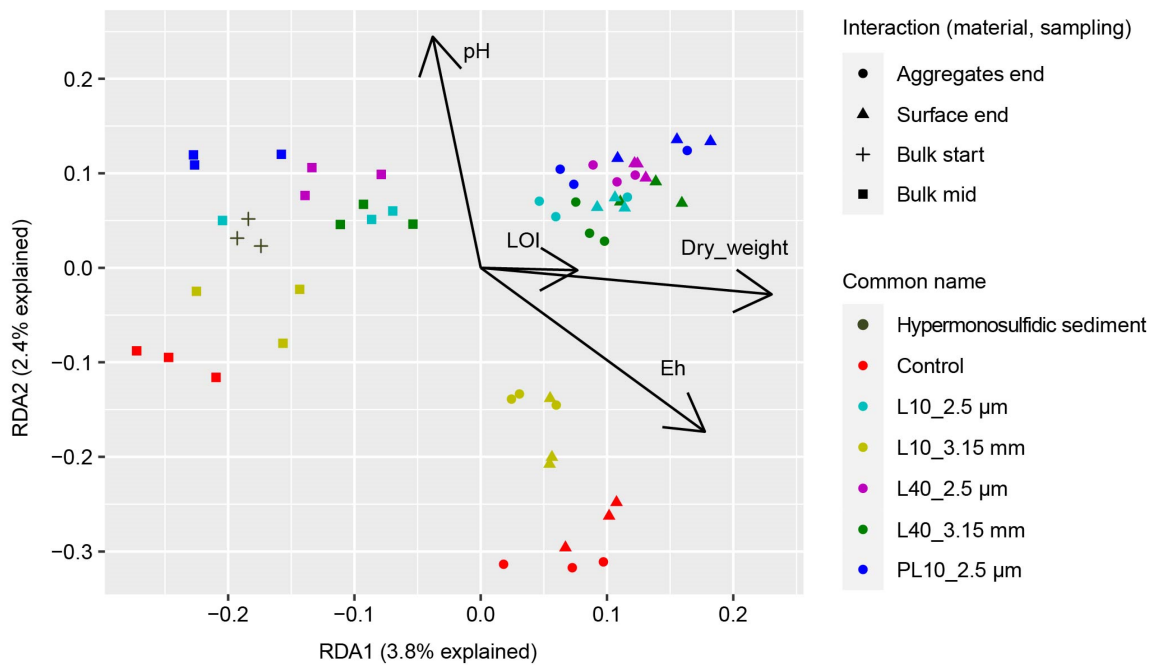


FIGURE 4 Redundancy analysis (RDA) of the microbial communities and key physicochemical parameters of the hypermonosulfidic sediment, the control, and the five treatments as well as the three sampling periods. LOI = loss on ignition generally representing organic matter.



FIGURE 5 Stacked bar graphs of the microbial community composition at the family level consisting of the top 20 respective taxa with 'Other' depicting the remaining diversity to make 100%. All samples are biological triplicate averages.

environment at 63° N. A second abundant population found belonged to the moderately acidophilic and sulfur oxidizing bacteria (SOB) Sulfuricellaceae (4.8%) genus *Sulfuricella*. In addition, Gallionellaceae (3.6%) were present that are mesophilic acid tolerant iron oxidizing bacteria (IOB) and SOB with genes coding for metal resistance mechanisms (Högfors-Rönnholm et al., 2022) and are known community members of acid sulfate soils in southern Sweden (Johnson et al., 2024) and Finland (Johnson et al., 2022). The populations further included the mesophilic IOB Burkholderiaceae (2.3%) that encompasses the genera *Acidovorax* and *Polaromonas* (Fan et al., 2021; Sun et al., 2020) and play a role in acid sulfate soils (Högfors-Rönnholm et al., 2022); the SRB Desulfurivibrionaceae (1.7%) genus *BM506* that is found in Arctic cold, anoxic, hypersaline alkaline springs (Magnuson et al., 2023) also likely reflecting the low temperature site where the sediment was sampled; and the SOB Halothiobacillaceae (1.0%) that grow at circumneutral pH values in Canadian acid mine drainage environments (Whaley-Martin et al., 2019) in line with the high pH and cold setting of the sediment. The remaining 'Other' populations composed 56%.

In the control mid sample (pH 6.5), the microbial community had changed and was now dominated by the SOB Halothiobacillaceae (30.7%). Further populations with high relative abundance included the IOB and SOB Gallionellaceae (13.9%), the SRB Desulfurivibrionaceae (10.1%), and the iron-reducing Holophagaceae (5.6%) (phylum Acidobacteriota, genus *Geothrix*; Coates, 1999). In contrast, the 34–128 and Sulfuricellaceae decreased in relative abundance (1.3% and 2.6%, respectively) compared with the hypermonosulfidic sediment (Figure 5). These changes were likely due to this sample including both oxidized and reduced sediment materials that certainly had different pH and Eh values selecting for various communities.

For the acidic control end sample (pH 3.3), the surface material was devoid of Halothiobacillaceae and Desulfurivibrionaceae, which likely have a growth optimum at mesophilic and circumneutral pH values (Magnuson et al., 2023; Whaley-Martin et al., 2019). Furthermore, there were differences between the surface and aggregates, where the surface had lower relative abundance of Gallionellaceae (1.6% and 20.2%, respectively) and higher relative abundances of Alicyclobacillaceae (22.9% and 0.6%, respectively). The latter is an acidophilic SOB (Yi et al., 2023). As Fe^{2+} was shown to migrate from the aggregates to the surfaces where the Fe was precipitated, the dominating Gallionellaceae population inside the aggregates likely acted as sulfur oxidizers (Högfors-Rönnholm et al., 2022) and thereby, oxidized the sulfur in the iron sulfides first although a lot of Fe^{2+} was present. The reason for this is probably due to the fact that

S oxidizes at lower redox conditions than Fe (Sposito, 2008), and is in contrast with studies on acidophilic microorganisms in biomining environments where ferrous iron is preferentially oxidized over sulfur (Liljeqvist et al., 2013). In contrast, the growth of the Alicyclobacillaceae population on the surfaces could have been stimulated due to the high total S concentrations and may further have been involved in the formation of secondary minerals (Yi et al., 2023), such as schwertmannite identified in this sample. Furthermore, the acidophilic Baltobacteraceae had high relative abundances in both surface and aggregates (8.1% and 8.4%). These three families have been previously identified in Antarctic soils (Ji et al., 2021), acid mine drainage environments (Williams et al., 2023), and Swedish acid sulfate soils (Johnson et al., 2024) that once again would have similar characteristics of low temperature. Furthermore, in the aggregates, there was a high relative abundance of Burkholderiaceae (Figure 5). Taken together, these results suggested ongoing oxidation and acidification, in agreement with a portion of the pyrite pool remaining (Table 2) and substantial leaching of sulfate (Figure 1d) related to both pyrite and AVS oxidation. Whereas the strong decrease in pH selected for acidophilic taxa, there was a lack of higher relative abundances of taxa frequently associated with acid sulfate soils of the colder higher Nordic latitudes, such as Ktedonobacteraceae, and showed instead taxa found in the warmer lower Nordic latitudes, such as Gallionellaceae (Johnson et al., 2024). This suggests a lower incubation temperature may have partly selected other acidophilic taxa. The presence of moderately acidophilic, acid tolerant, SOB and IOB populations in the near-neutral and anoxic hypermonosulfidic sediment together with the notable increase of these populations during incubation suggested that they had the ability to rapidly increase in both abundance and metabolic activity in response to environmental changes (Ling et al., 2018), in this case an increase in oxygen availability, a strong decrease in pH, and the incubation temperature used.

For L10_{3,15 mm} treatment, there was a lack of high relative abundance of acidophilic communities. The pH of the mid sample had dropped to 7.3 (Figure 2a), and in the drainage water the sulfate concentrations were high (Figure 1d), which was evidence of ongoing iron-sulfide oxidation. It is likely that Fe oxidation was due to the activity of the dominating Burkholderiaceae (36.0%), while sulfur cycling was likely mediated by Desulfurivibrionaceae (11.1%), Gallionellaceae (10.3%) and Sulfuricellaceae (8.9%). In the end samples, where the pH had decreased to 4.9 in the surface and to 5.5 in the aggregates (Figure 2a), the acid-tolerant denitrifier, Rhodanobacteraceae (Green et al., 2012), which are known community members of acid sulfate soils (Högfors-Rönnholm et al., 2020; Johnson

et al., 2022) and involved in thiosulfate oxidation (Högfors-Rönholm et al., 2022), dominated in the surface (24.9%) and was also quite abundant in the aggregates (7.8%). There were also high relative abundances of Gallionellaceae (aggregates: 23.5% and surface: 9.5%) and Burkholderiaceae (aggregates: 9.3% and surface: 6.2%). Sulfuricellaceae relative abundances strongly decreased (compared with the mid sample) at both the surface and aggregates (0.4% and 3.6%, respectively) as did Desulfurivibrionaceae (0.2% and 2.3%, respectively) (Figure 5). The decrease in relative abundance of these two SOBs correlated with the decrease in pH in the samples; namely, higher abundances at pH values >5 and negligible abundances at pH values <5, which reflects the pH optima for species in the Sulfuricellaceae (Hayakawa et al., 2021) and Desulfurivibrionaceae (Magnuson et al., 2023) families. In the aggregates, the dominance of the Gallionellaceae family followed by lower relative abundances of a more mixed community of IOBs, SOBs and SRBs suggested that sulfur and iron cycling were ongoing. In the surface, in contrast, Rhodanobacteraceae may have been involved in the sulfur cycling. These features reflected the changing geochemical environment in the L10_{3.15 mm} treatment over time, with a decreasing soil pH both in surfaces and aggregates (Figure 2), AVS being oxidized but pyrite partly remaining in the aggregates (Table 2) and high sulfate concentrations in the drainage waters (Figure 1d).

For L10_{2.5 μm}, PL10_{2.5 μm}, L40_{3.15 mm} and L40_{2.5 μm}, which maintained a pH between 7.8 and 8.1 (Figure 2), the developed microbial communities had many features in common and were also similar to L10_{3.15 mm} with the increasing relative abundances of IOB and SOBs and still having some presence of SRBs. The end sampling showed the greatest differences from the control and the mid sampling. The L40_{3.15 mm} surface showed a dominance of Sphingomonadaceae (21.4%) that is a mesophilic SOB previously utilized in experiments to mobilize Cd contamination (Wang et al., 2021), along with a more mixed community of SOBs and IOBs. In the L40_{3.15 mm} aggregates, Sphingomonadaceae occurred at only 0.7% and was replaced with the IOB and SOB Gallionellaceae (14.5%), the IOB Burkholderiaceae (15.9%), as well as the SOB Desulfocapsaceae (0.6%) that has previously been identified in Arctic marine sediments (Begmatov et al., 2021). The dominance of these species in the aggregates indicated an ongoing sulfur and iron oxidation at a neutral pH value which can also be seen as a decrease in the AVS pool in the aggregates and enrichment of sulfur in the surface (Table 2). For L10_{2.5 μm}, L40_{2.5 μm}, and PL10_{2.5 μm}, the end-sample surface communities were generally composed of the same taxa. However, L10_{2.5 μm} was dominated by Burkholderiaceae; PL10_{2.5 μm} by A4b (of phylum Chloroflexota, class Anaerolineae, order SBR1031) that has

been identified in Swedish acid-sulfate soils (Johnson et al., 2024); and L40_{2.5 μm} by Cyclobacteriaceae found in the upper sediments of the Barents Sea, and may be involved in methane, sulfur and nitrogen cycling (Begmatov et al., 2021), along with Gallionellaceae. The Anaerolineae are known to be able to degrade cellulose (Xia et al., 2016), and this could be the reason for the dominance of the A4b family in the PL10_{2.5 μm} treatment, whereas the A4b only showed negligible abundances in the other treatments lacking a cellulose source (Figure 5). The aggregate communities of these treatments showed more community dissimilarity. L10_{2.5 μm} was dominated by Gallionellaceae, Burkholderiaceae and Desulfurivibrionaceae; L40_{2.5 μm} was dominated by Gallionellaceae, Burkholderiaceae and Sphingomonadaceae; and PL10_{2.5 μm} was dominated by Burkholderiaceae and Desulfocapsaceae. All these represent, however, communities with iron and sulfur oxidizing capacities at neutral pH values, and most of them were identified at lower relative abundances in the hypermonosulfidic sediment, except for Sphingomonadaceae and Desulfocapsaceae that were identified also in the L40_{3.15 mm} treatment. Sphingomonadaceae was only identified in the L40_{3.15 mm} and L40_{2.5 μm} treatments that had the highest Ca concentrations in the surface and aggregates of all treatments (Table 1). As Sphingomonadaceae has been identified in drip water from limestone caves (Marques et al., 2019), the high Ca concentration in these treatments could be an indication as to why these treatments were selected for this microbial community. In conclusion, the acidity-neutralizing effects of the limestone and availability of organic matter from the peat additions on the microbial community inhibited the development of extreme SOB and IOB acidophiles implicated in acidity generation, such as Alicyclobacillaceae and Baltobacteraceae identified in the acidic control. However, the continued development of taxa capable of neutrophilic sulfur and iron oxidation were not inhibited and thus facilitated ongoing iron sulfide oxidation and sulfate leaching in spite of high pH.

4 | CONCLUSIONS

Overall, the limestone treatments of the incubated hypermonosulfidic sediment decelerated pyrite oxidation, slowed down the movement of the oxidation front (more extensive residues), strongly minimized the formation of dissolved and solid-phase labile Al, and caused formation of gypsum as well as secondary Fe(III) phases more labile (increased extractability with 0.25 M hydroxylamine hydrochloride) than corresponding Fe phases formed in the control. In terms of pH, applying limestone in doses corresponding to the theoretical acidity produced by

sulfide oxidation did not prevent a pH drop to sub-5.0 levels when a coarse-grained variant was used (particles <3.15 mm, and half of them <0.80 mm), but kept the pH near neutral when a fine-grained variant was used (median grain size of 2.5 μm). This showed that decreasing the grain size and thus, increasing the surface area of the limestone particles was positive in terms of hindering acidity formation. The severe decrease in pH in the control selected for acidophilic taxa, while the high pH in the treatments was in congruence with the absence of acidophiles along with the presence and high relative abundances of both SOBs and IOBs. This showed that microbial communities that developed within the limestone treatments sustained iron-sulfide oxidation despite the high pH, in line with the geochemical data showing a nearly complete oxidation of the metastable iron sulfides, but still with large pools of pyrite present.

AUTHOR CONTRIBUTIONS

Liubov Kononova: Methodology; investigation; validation; writing – original draft; writing – review and editing; visualization. **Anders Johnson:** Methodology; investigation; validation; writing – original draft; writing – review and editing; visualization. **Sten Engblom:** Conceptualization; methodology; investigation; funding acquisition; writing – review and editing. **Pekka Stén:** Conceptualization; methodology; investigation; funding acquisition. **Changxun Yu:** Conceptualization; writing – review and editing. **Peter Österholm:** Conceptualization; methodology; writing – review and editing. **Vadim Kessler:** Writing – review and editing; investigation; methodology. **Gulaim Seisenbaeva:** Writing – review and editing; methodology; investigation. **Mark Dopson:** Conceptualization; writing – review and editing; supervision. **Mats Åström:** Conceptualization; funding acquisition; writing – review and editing; supervision. **Eva Högfors-Rönholm:** Conceptualization; methodology; investigation; funding acquisition; project administration; writing – review and editing.

ACKNOWLEDGEMENTS

We thank Fanny Ahonen and Jarkko Linnamaa at Åbo Akademi University for the sulfur speciation analyses and Krister Dalhem at Novia University of Applied Sciences for constructive comments.

FUNDING INFORMATION

We acknowledge the financial support by the European Regional Development Fund via the Interreg Botnia-Atlantica program to the project ‘Sustainable treatment of coastal deposited sulfide soils’ (STASIS; project ID 20203245) and via the Interreg Aurora program to the project ‘Best practices for sustainable stabilisation and reuse of sulfidic soils with minimised environmental impact’ (MinImpact;

project ID 20361791). S.E. and E.H.-R. further acknowledges Maa- ja Vesitekniiikan Tuki Ry for additional financial support (grant number 45971). M.D. further acknowledges the Science for Life Laboratory (SciLifeLab) and the National Genomics Infrastructure (NGI). Bioinformatics analyses were carried out utilizing the Uppsala Multidisciplinary Center for Advanced Computational Science (UPPMAX) at Uppsala University (projects NAISS 2023/22-893 and 2023/6-261). The computations were enabled by resources provided by the National Academic Infrastructure for Supercomputing in Sweden (NAISS) and the Swedish National Infrastructure for Computing (SNIC) at UPPMAX, Uppsala University partially funded by the Swedish Research Council through grant agreement nos. 2022-06725 and 2018-05973.

DATA AVAILABILITY STATEMENT

16S rRNA gene sequences are available in the European nucleotide archive study reference under the BioProject accession number: PRJEB72671 and sample accession numbers: ERS18284095 through ERS18284154. Microbiological data analysis and Figures were prepared in R and the full reproducible code is available in SI4.

ORCID

Liubov Kononova  <https://orcid.org/0009-0000-2610-0032>

Anders Johnson  <https://orcid.org/0000-0003-2943-5158>

Sten Engblom  <https://orcid.org/0000-0001-7334-5622>

Changxun Yu  <https://orcid.org/0000-0002-0635-3718>

Vadim Kessler  <https://orcid.org/0000-0001-7570-2814>

Gulaim Seisenbaeva  <https://orcid.org/0000-0003-0072-6082>

Mark Dopson  <https://orcid.org/0000-0002-9622-3318>

Mats Åström  <https://orcid.org/0000-0002-3585-2209>

Eva Högfors-Rönholm  <https://orcid.org/0000-0002-2520-4662>

REFERENCES

- Aitchison, J. (1982). The statistical analysis of compositional data. *Journal of the Royal Statistical Society, Series B (Methodological)*, 44, 139–177.
- Andriessse, J. P. (1988). *Nature and management of tropical peat soils*. Food and Agriculture Organization of the United Nations.
- Arkesteyn, G. J. M. W. (1980). Pyrite oxidation in acid sulphate soils: The role of microorganisms. *Plant and Soil*, 54, 119–134. <https://doi.org/10.1007/BF02182004>
- Åström, M., & Björklund, A. (1997). Geochemistry and acidity of sulphide-bearing postglacial sediments of western Finland. *Environmental Geochemistry and Health*, 19, 155–164.
- Åström, M., Österholm, P., Bärlund, I., & Tattari, S. (2007). Hydrochemical effects of surface liming, controlled drainage and lime-filter drainage on boreal acid sulfate soils. *Water, Air, and Soil Pollution*, 179, 107–116. <https://doi.org/10.1007/s11270-006-9217-8>

- Åström, M. E., Österholm, P., Gustafsson, J. P., Nystrand, M., Peltola, P., Nordmyr, L., & Boman, A. (2012). Attenuation of rare earth elements in a boreal estuary. *Geochimica et Cosmochimica Acta*, 96, 105–119. <https://doi.org/10.1016/j.gca.2012.08.004>
- Bärlund, I., Tattari, S., Yli-Halla, M., & Åström, M. (2005). Measured and simulated effects of sophisticated drainage techniques on groundwater level and runoff hydrochemistry in areas of boreal acid sulphate soils. *Agricultural and Food Science*, 14, 98–111.
- Begmatov, S., Savvichev, A. S., Kadnikov, V. V., Beletsky, A. V., Rusanov, I. I., Klyuvitkin, A. A., Novichkova, E. A., Mardanov, A. V., Pimenov, N. V., & Ravin, N. V. (2021). Microbial communities involved in methane, sulfur, and nitrogen cycling in the sediments of the Barents Sea. *Microorganisms*, 9, 2362. <https://doi.org/10.3390/microorganisms9112362>
- Ben Ahmed, S., Tlili, M. M., Amami, M., & Ben Amor, M. (2014). Gypsum precipitation kinetics and solubility in the NaCl–MgCl₂–CaSO₄–H₂O system. *Industrial and Engineering Chemistry Research*, 53, 9554–9560. <https://doi.org/10.1021/ie5004224>
- Björkqvist, D., & Weppling, K. (1987). Liming as a method to neutralize highly acidic drainage waters from sulphate basins in western Finland. Proceedings of the International Symposium on Acidification and Water Pathways.
- Boesen, C., & Postma, D. (1988). Pyrite formation in anoxic environments of the Baltic. *American Journal of Science*, 288, 575–603.
- Bolyen, E., Rideout, J. R., Dillon, M. R., Bokulich, N. A., Abnet, C. C., Al-Ghalith, G. A., Alexander, H., Alm, E. J., Arumugam, M., Asnicar, F., Bai, Y., Bisanz, J. E., Bittinger, K., Brejnrod, A., Brislawn, C. J., Brown, C. T., Callahan, B. J., Caraballo-Rodríguez, A. M., Chase, J., ... Caporaso, J. G. (2019). Reproducible, interactive, scalable and extensible microbiome data science using QIIME 2. *Nature Biotechnology*, 37, 852–857. <https://doi.org/10.1038/s41587-019-0209-9>
- Boman, A., Åström, M., & Fröjdö, S. (2008). Sulfur dynamics in boreal acid sulfate soils rich in metastable iron sulfide—The role of artificial drainage. *Chemical Geology*, 255, 68–77. <https://doi.org/10.1016/j.chemgeo.2008.06.006>
- Boman, A., Fröjdö, S., Backlund, K., & Åström, M. (2010). Impact of isostatic land uplift and artificial drainage on oxidation of brackish-water sediments rich in metastable iron sulfide. *Geochimica et Cosmochimica Acta*, 74, 1268–1281. <https://doi.org/10.1016/j.gca.2009.11.026>
- Boman, A., Mattbäck, S., Becher, M., Yli-Halla, M., Sohlenius, G., Auri, J., Öhring, C., Liwata-Kenttälä, P., & Edén, P. (2023). Classification of acid sulfate soils and soil materials in Finland and Sweden: Re-introduction of para-acid sulfate soils. *Bulletin of the Geological Society of Finland*, 95, 161–186. <https://doi.org/10.17741/bgsf/95.2.004>
- Caldeira, C. L., Ciminelli, V. S. T., Dias, A., & Osseo-Asare, K. (2003). Pyrite oxidation in alkaline solutions: Nature of the product layer. *International Journal of Mineral Processing*, 72, 373–386. [https://doi.org/10.1016/S0301-7516\(03\)00112-1](https://doi.org/10.1016/S0301-7516(03)00112-1)
- Callahan, B. J., McMurdie, P. J., Rosen, M. J., Han, A. W., Johnson, A. J. A., & Holmes, S. P. (2016). DADA2: High-resolution sample inference from Illumina amplicon data. *Nature Methods*, 13, 581–583. <https://doi.org/10.1038/nmeth.3869>
- Cappuyns, V., & Swennen, R. (2008). The application of pHstat leaching tests to assess the pH-dependent release of trace metals from soils, sediments and waste materials. *Journal of Hazardous Materials*, 158, 185–195. <https://doi.org/10.1016/j.jhazmat.2008.01.058>
- Chan, K. Y., & Heenan, D. P. (1999). Lime-induced loss of soil organic carbon and effect on aggregate stability. *Soil Science Society of America Journal*, 63, 1841–1844. <https://doi.org/10.2136/sssaj1999.6361841x>
- Chen, Q., Cohen, D. R., Andersen, M. S., Robertson, A. M., & Jones, D. R. (2022). Stability and trace element composition of natural schwertmannite precipitated from acid mine drainage. *Applied Geochemistry*, 143, 105370. <https://doi.org/10.1016/j.apgeochem.2022.105370>
- Christel, S., Yu, C., Wu, X., Josefsson, S., Lillhonga, T., Högfors-Rönholm, E., Sohlenius, G., Åström, M. E., & Dopson, M. (2019). Comparison of boreal acid sulfate soil microbial communities in oxidative and reductive environments. *Research in Microbiology*, 170, 288–295. <https://doi.org/10.1016/j.resmic.2019.06.002>
- Coates, J. D. (1999). *Geothrix ferrnentans* gen. nov., sp. nov., a novel Fe(III)-reducing bacterium from a hydrocarbon-contaminated aquifer. *International Journal of Systematic Bacteriology*, 49, 1615–1622.
- Collins, R. N., Jones, A. M., & Waite, T. D. (2010). Schwertmannite stability in acidified coastal environments. *Geochimica et Cosmochimica Acta*, 74, 482–496. <https://doi.org/10.1016/j.gca.2009.10.014>
- Dalhem, K., Mattbäck, S., Boman, A., & Österholm, P. (2021). A simplified distillation-based sulfur speciation method for sulfidic soil materials. *Bulletin of the Geological Society of Finland*, 93, 19–30. <https://doi.org/10.17741/bgsf/93.1.002>
- Dong, X., Zhang, C., Peng, Y., Zhang, H.-X., Shi, L.-D., Wei, G., Hubert, C. R. J., Wang, Y., & Greening, C. (2022). Phylogenetically and catabolically diverse diazotrophs reside in deep-sea cold seep sediments. *Nature Communications*, 13, 4885. <https://doi.org/10.1038/s41467-022-32503-w>
- Dopson, M., Ossandon, F. J., Lövgren, L., & Holmes, D. S. (2014). Metal resistance or tolerance? Acidophiles confront high metal loads via both abiotic and biotic mechanisms. *Frontiers in Microbiology*, 5, 00157. <https://doi.org/10.3389/fmicb.2014.00157>
- Eberle, A., Besold, J., León Ninin, J. M., Kerl, C. F., Kujala, K., & Planer-Friedrich, B. (2021). Potential of high pH and reduced sulfur for arsenic mobilization – Insights from a Finnish peatland treating mining waste water. *Science of the Total Environment*, 758, 143689. <https://doi.org/10.1016/j.scitotenv.2020.143689>
- Edén, P., Boman, A., Mattbäck, S., Auri, J., Yli-Halla, M., & Österholm, P. (2023). Mapping, impacts, characterization and extent of acid sulfate soils in Finland. *Bulletin of the Geological Society of Finland*, 95, 135–160. <https://doi.org/10.17741/bgsf/95.2.003>
- Edén, P., Weppling, K., & Jokela, S. (1999). Natural and land-use induced load of acidity, metals, humus and suspended matter in Lestijoki, a river in western Finland. *Boreal Environment Research*, 4, 31–43.
- Enio, M. S. K., Shamshuddin, J., Fauziah, C. I., Husni, M. H. A., & Panhwar, Q. A. (2020). Quantifying the release of acidity and metals arising from drainage of acid sulfate soils in the Kelantan Plains, Malaysia. *Mining of Mineral Deposits*, 14, 50–60. <https://doi.org/10.33271/mining14.03.050>

- Ezzaim, A., Turpault, M.-P., & Ranger, J. (1999). Quantification of weathering processes in an acid brown soil developed from tuff (Beaujolais, France): Part II. Soil formation. *Geoderma*, 87, 155–177.
- Fan, X., Xing, X., & Ding, S. (2021). Enhancing the retention of phosphorus through bacterial oxidation of iron or sulfide in the eutrophic sediments of Lake Taihu. *Science of the Total Environment*, 791, 148039. <https://doi.org/10.1016/j.scitotenv.2021.148039>
- Fitzpatrick, R. W., Mosley, L. M., Raven, M. D., & Shand, P. (2017). Schwertmannite formation and properties in acidic drain environments following exposure and oxidation of acid sulfate soils in irrigation areas during extreme drought. *Geoderma*, 308, 235–251. <https://doi.org/10.1016/j.geoderma.2017.08.012>
- Gill, R. (Ed.). (1997). Modern analytical geochemistry: an introduction to quantitative chemical analysis techniques for earth, environmental and materials scientists, Transferred to digital print on demand. ed, Geochemistry series. Longman, Harlow.
- Goodman, A. J., Scircle, A., Kimble, A., Harris, W., Calvitti, B., Sirkis, D., Mathurin, L., Grassi, V., Ranville, J. F., & Bednar, A. J. (2023). Critical metal geochemistry in groundwaters influenced by dredged material. *Science of the Total Environment*, 884, 163725. <https://doi.org/10.1016/j.scitotenv.2023.163725>
- Green, S. J., Prakash, O., Jasrotia, P., Overholt, W. A., Cardenas, E., Hubbard, D., Tiedje, J. M., Watson, D. B., Schadt, C. W., Brooks, S. C., & Kostka, J. E. (2012). Denitrifying bacteria from the genus *Rhodanobacter* dominate bacterial communities in the highly contaminated subsurface of a nuclear legacy waste site. *Applied and Environmental Microbiology*, 78, 1039–1047. <https://doi.org/10.1128/AEM.06435-11>
- Hadzic, M., Postila, H., Österholm, P., Nystrand, M., Pahkakangas, S., Karppinen, A., Arola, M., Nilivaara-Koskela, R., Häkkinen, K., & Saukkoriipi, J. (2014). Sulfaattimailla syntyvän happaman kuormituksen ennakointi- ja hallintamenetelmät. *Suomen ympäristökeskuksen raportteja*, 17.
- Hall, G. E. M. (1998). Analytical perspective on trace element species of interest in exploration. *Journal of Geochemical Exploration*, 61, 1–19.
- Hall, G. E. M., Vaive, J. E., Beer, R., & Hoashi, M. (1996). Selective leaches revisited, with emphasis on the amorphous Fe oxyhydroxide phase extraction. *Journal of Geochemical Exploration*, 56, 59–78. [https://doi.org/10.1016/0375-6742\(95\)00050-X](https://doi.org/10.1016/0375-6742(95)00050-X)
- Hall, G. E. M., Vaive, J. E., & MacLaurin, A. I. (1996). Analytical aspects of the application of sodium pyrophosphate reagent in the specific extraction of the labile organic component of humus and soils. *Journal of Geochemical Exploration*, 56, 23–36. [https://doi.org/10.1016/0375-6742\(95\)00046-1](https://doi.org/10.1016/0375-6742(95)00046-1)
- Hayakawa, A., Ota, H., Asano, R., Murano, H., Ishikawa, Y., & Takahashi, T. (2021). Sulfur-based denitrification in stream-bank subsoils in a headwater catchment underlain by marine sedimentary rocks in Akita, Japan. *Frontiers in Environmental Science*, 9, 664488. <https://doi.org/10.3389/fenvs.2021.664488>
- Herlemann, D. P., Labrenz, M., Jürgens, K., Bertilsson, S., Waniek, J. J., & Andersson, A. F. (2011). Transitions in bacterial communities along the 2000 km salinity gradient of the Baltic Sea. *The ISME Journal*, 5, 1571–1579. <https://doi.org/10.1038/ismej.2011.41>
- Högfors-Rönholm, E., Christel, S., Engblom, S., & Dopson, M. (2018). Indirect DNA extraction method suitable for acidic soil with high clay content. *MethodsX*, 5, 136–140. <https://doi.org/10.1016/j.mex.2018.02.005>
- Högfors-Rönholm, E., Christel, S., Lillhonga, T., Engblom, S., Österholm, P., & Dopson, M. (2020). Biodegraded peat and ultrafine calcium carbonate result in retained metals and higher microbial diversities in boreal acid sulfate soil. *Soil Ecology Letters*, 2, 120–130. <https://doi.org/10.1007/s42832-020-0039-1>
- Högfors-Rönholm, E., Lundin, D., Brambilla, D., Christel, S., Lopez-Fernandez, M., Lillhonga, T., Engblom, S., Österholm, P., & Dopson, M. (2022). *Gallionella* and *Sulfuricella* populations are dominant during the transition of boreal potential to actual acid sulfate soils. *Communications Earth & Environment*, 3, 304. <https://doi.org/10.1038/s43247-022-00642-z>
- Hugerth, L. W., Wefer, H. A., Lundin, S., Jakobsson, H. E., Lindberg, M., Rodin, S., Engstrand, L., & Andersson, A. F. (2014). DegePrime, a program for degenerate primer design for broad-taxonomic-range PCR in microbial ecology studies. *Applied and Environmental Microbiology*, 80, 5116–5123. <https://doi.org/10.1128/AEM.01403-14>
- Jeanroy, B. E., & Guillet, B. (1981). The occurrence of suspended ferruginous particles in pyrophosphate extracts of some soil horizons. *Geoderma*, 26, 95–105.
- Ji, M., Williams, T. J., Montgomery, K., Wong, H. L., Zaugg, J., Berengut, J. F., Bissett, A., Chuvochina, M., Hugenholtz, P., & Ferrari, B. C. (2021). *Candidatus Eremiobacterota*, a metabolically and phylogenetically diverse terrestrial phylum with acid-tolerant adaptations. *The ISME Journal*, 15, 2692–2707. <https://doi.org/10.1038/s41396-021-00944-8>
- Johnson, A., Högfors-Rönholm, E., Engblom, S., Österholm, P., Åström, M., & Dopson, M. (2022). Dredging and deposition of metal sulfide rich river sediments results in rapid conversion to acid sulfate soil materials. *Science of the Total Environment*, 813, 151864. <https://doi.org/10.1016/j.scitotenv.2021.151864>
- Johnson, A., Nyman, A., Åström, M., & Dopson, M. (2024). Regional variation in Swedish acid sulfate soil microbial communities is influenced by temperature and geochemistry. *European Journal of Soil Science*, 75, e13452. <https://doi.org/10.1111/ejss.13452>
- Joukainen, S., & Yli-Halla, M. (2003). Environmental impacts and acid loads from deep sulfidic layers of two well-drained acid sulfate soils in western Finland. *Agriculture, Ecosystems and Environment*, 95, 297–309. [https://doi.org/10.1016/S0167-8809\(02\)00094-4](https://doi.org/10.1016/S0167-8809(02)00094-4)
- Kaurichev, I. S., & Shishova, V. S. (1967). Oxidation reduction conditions of coarse textured soils of the Meschera lowland. *Soviet Soil Science*, 5, 636–646.
- Kronberg, T., Tarvainen, T., Auri, J., Eriksson, J.-E., Mattbäck, S., & Boman, A. (2024). Applying industrial side streams in the neutralization of acid generating sulfide-rich sediments – The impact on pH and leaching of harmful elements. *Journal of Geochemical Exploration*, 257, 107384. <https://doi.org/10.1016/j.gexplo.2023.107384>
- Lakanen, E., & Erviö, R. (1971). A comparison of eight extractants for the determination of plant available micronutrients in soils. *Acta Agriculturae Fenniae*, 123, 223–232.
- Liljeqvist, M., Rzhepishevskaya, O. I., & Dopson, M. (2013). Gene identification and substrate regulation provide insights into sulfur accumulation during bioleaching with the psychrotolerant acidophile *Acidithiobacillus ferrivorans*. *Applied and Environmental Microbiology*, 79, 951–957. <https://doi.org/10.1128/AEM.02989-12>

- Lindgren, A., Jonasson, I. K., Öhrling, C., & Giese, M. (2022). Acid sulfate soils and their impact on surface water quality on the Swedish west coast. *Journal of Hydrology: Regional Studies*, 40, 101019. <https://doi.org/10.1016/j.ejrh.2022.101019>
- Ling, Y.-C., Gan, H. M., Bush, M., Bush, R., & Moreau, J. W. (2018). Time-resolved microbial guild responses to tidal cycling in a coastal acid-sulfate system. *Environment and Chemistry*, 15, 2. <https://doi.org/10.1071/EN16203>
- Magnuson, E., Altshuler, I., Freyria, N. J., Leveille, R. J., & Whyte, L. G. (2023). Sulfur-cycling chemolithoautotrophic microbial community dominates a cold, anoxic, hypersaline Arctic spring. *Microbiome*, 11, 203. <https://doi.org/10.1186/s40168-023-01628-5>
- Marques, E. L. S., Silva, G. S., Dias, J. C. T., Gross, E., Costa, M. S., & Rezende, R. P. (2019). Cave drip water-related samples as a natural environment for aromatic hydrocarbon-degrading bacteria. *Microorganisms*, 7, 33. <https://doi.org/10.3390/microorganisms7020033>
- Mattbäck, S., Boman, A., Sandfält, A., & Österholm, P. (2022). Leaching of acid generating materials and elements from coarse- and fine-grained acid sulfate soil materials. *Journal of Geochemical Exploration*, 232, 106880. <https://doi.org/10.1016/j.gexplo.2021.106880>
- McMurdie, P. J., & Holmes, S. (2014). Waste not, want not: Why rarefying microbiome data is inadmissible. *PLoS Computational Biology*, 10, e1003531. <https://doi.org/10.1371/journal.pcbi.1003531>
- Niemela, S. I., & Tuovinen, O. H. (1972). Acidophilic thiobacilli in the river Sirppujoki. *Journal of General Microbiology*, 73, 23–28. <https://doi.org/10.1099/00221287-73-1-23>
- Nordmyr, L., Åström, M., & Peltola, P. (2008). Metal pollution of estuarine sediments caused by leaching of acid sulphate soils. *Estuarine, Coastal and Shelf Science*, 76, 141–152. <https://doi.org/10.1016/j.ecss.2007.07.002>
- Nyman, A., Johnson, A., Yu, C., Sohlenius, G., Becher, M., Dopson, M., & Åström, M. (2023). A nationwide acid sulfate soil study—A rapid and cost-efficient approach for characterizing large-scale features. *Science of the Total Environment*, 869, 161845. <https://doi.org/10.1016/j.scitotenv.2023.161845>
- Nystrand, M. I., Hadzic, M., Postila, H., Wichmann, A., Karppinen, A., Ihme, R., & Österholm, P. (2021). Characteristics of sulfide bearing soil materials in peat extraction areas in N-Finland. *Journal of Geochemical Exploration*, 220, 106640. <https://doi.org/10.1016/j.gexplo.2020.106640>
- Oksanen, J., Blanchet, F. G., Friendly, M., Kindt, R., Legendre, P., McGlinn, D., Minchin, P. R., O'Hara, R. B., Simpson, G. L., Solymos, P., Stevens, M. H. H., Szoecs, E., & Wagner, H. (2020). Package. R package version 2.5-7. *vegan: Community Ecology*.
- Österholm, P., & Åström, M. (2002). Spatial trends and losses of major and trace elements in agricultural acid sulphate soils distributed in the artificially drained Rintala area, W. Finland. *Applied Geochemistry*, 17, 1209–1218. [https://doi.org/10.1016/S0883-2927\(01\)00133-0](https://doi.org/10.1016/S0883-2927(01)00133-0)
- Österholm, P., Virtanen, S., Rosendahl, R., Uusi-Kämpä, J., Ylivainio, K., Yli-Halla, M., Mäensivu, M., & Turtola, E. (2015). Groundwater management of acid sulfate soils using controlled drainage, by-pass flow prevention, and subsurface irrigation on a boreal farmland. *Acta Agriculturae Scandinavica, Section B—Soil and Plant Science*, 65, 110–120. <https://doi.org/10.1080/09064710.2014.997787>
- Parks, D. H., Rinke, C., Chuvochina, M., Chaumeil, P.-A., Woodcroft, B. J., Evans, P. N., Hugenholtz, P., & Tyson, G. W. (2017). Recovery of nearly 8,000 metagenome-assembled genomes substantially expands the tree of life. *Nature Microbiology*, 2, 1533–1542. <https://doi.org/10.1038/s41564-017-0012-7>
- Peltola, P., & Åström, M. (2002). Concentrations and leachability of chemical elements in estuarine sulfur-rich sediments, W. Finland. *Science of the Total Environment*, 284, 109–122. [https://doi.org/10.1016/S0048-9697\(01\)00872-5](https://doi.org/10.1016/S0048-9697(01)00872-5)
- Quast, C., Pruesse, E., Yilmaz, P., Gerken, J., Schweer, T., Yarza, P., Peplies, J., & Glöckner, F. O. (2012). The SILVA ribosomal RNA gene database project: Improved data processing and web-based tools. *Nucleic Acids Research*, 41, D590–D596. <https://doi.org/10.1093/nar/gks1219>
- R Core Team. (2019). *A language and environment for statistical computing*. R Foundation for Statistical Computing.
- Rickard, D., & Morse, J. W. (2005). Acid volatile sulfide (AVS). *Marine Chemistry*, 97, 141–197. <https://doi.org/10.1016/j.marchem.2005.08.004>
- Saarinen, T., Mohämmädighävam, S., Marttila, H., & Kløve, B. (2013). Impact of peatland forestry on runoff water quality in areas with sulphide-bearing sediments; how to prevent acid surges. *Forest Ecology and Management*, 293, 17–28. <https://doi.org/10.1016/j.foreco.2012.12.029>
- Salminen, R., Batista, M. J., Bidovec, M., Demetriades, A., De Vivo, B., De Vos, W., Đuriš, M., Gilucis, A., Gregorauskiene, V., Halamić, J., Heitzmann, P., Lima, A., Jordan, G., Klaver, J., Klein, P., Lis, J., Locutura, J., Marsina, K., Mazreku, A., ... Tarvainen, T. (2005). *Geochemical Atlas of Europe*. Geological Survey of Finland.
- Salo, H., Virtanen, S., Laine-Kaulio, H., Koivusalo, H., Jacques, D., & Kokkonen, T. (2023). Evolution of pH, redox potential and solute concentrations in soil and drainage water at a cultivated acid sulfate soil profile. *Geoderma*, 436, 116559. <https://doi.org/10.1016/j.geoderma.2023.116559>
- Schoepfer, V. A., & Burton, E. D. (2021). Schwertmannite: A review of its occurrence, formation, structure, stability and interactions with oxyanions. *Earth Science Reviews*, 221, 103811. <https://doi.org/10.1016/j.earscirev.2021.103811>
- Shahabi-Ghahfarokhi, S., Åström, M., Yu, C., Lindquist, T., Djerf, H., Kalbitz, K., & Ketzer, M. (2022). Extensive dispersion of metals from hemiboreal acid sulfate soil into adjacent drain and wetland. *Applied Geochemistry*, 136, 105170. <https://doi.org/10.1016/j.apgeochem.2021.105170>
- Shotyk, W. (1988). Review of the inorganic geochemistry of peats and peatland waters. *Earth Science Reviews*, 25, 95–176. [https://doi.org/10.1016/0012-8252\(88\)90067-0](https://doi.org/10.1016/0012-8252(88)90067-0)
- Slonczewski, J. L., Fujisawa, M., Dopson, M., & Krulwich, T. A. (2009). Cytoplasmic pH measurement and homeostasis in bacteria and archaea. In *Advances in microbial physiology* (pp. 1–317). Elsevier. [https://doi.org/10.1016/S0065-2911\(09\)05501-5](https://doi.org/10.1016/S0065-2911(09)05501-5)
- Sposito, G. (2008). *The chemistry of soils* (Second ed.). Oxford university press.
- Straub, D., Blackwell, N., Langarica-Fuentes, A., Peltzer, A., Nahnsen, S., & Kleindienst, S. (2020). Interpretations of environmental microbial community studies are biased by the selected 16S rRNA (gene) amplicon sequencing pipeline. *Frontiers in Microbiology*, 11, 550420. <https://doi.org/10.3389/fmicb.2020.550420>
- Sukitprapanon, T., Suddhiprakarn, A., Kheoruenromne, I., & Gilkes, R. J. (2018). Partitioning and potential mobilization of aluminum, arsenic, iron, and heavy metals in tropical active and post-active acid sulfate soils: Influence of long-term paddy rice cultivation. *Chemosphere*, 197, 691–702. <https://doi.org/10.1016/j.chemosphere.2018.01.099>

- Sun, X., Qiu, L., Kolton, M., Häggblom, M., Xu, R., Kong, T., Gao, P., Li, B., Jiang, C., & Sun, W. (2020). V^V reduction by *Polaromonas* spp. in vanadium mine tailings. *Environmental Science & Technology*, 54, 14442–14454. <https://doi.org/10.1021/acs.est.0c05328>
- Toivonen, J., Hudd, R., Nystrand, M., & Österholm, P. (2020). Climatic effects on water quality in areas with acid sulfate soils with commensurable consequences on the reproduction of burbot (*Lota lota* L.). *Environmental Geochemistry and Health*, 42, 3141–3156. <https://doi.org/10.1007/s10653-020-00550-1>
- Uhlmann, W., Büttcher, H., Totsche, O., & Steinberg, C. E. W. (2004). Buffering of acidic mine lakes: The relevance of surface exchange and solid-bound Sulphate. *Mine Water and the Environment*, 23, 20–27. <https://doi.org/10.1007/s10230-004-0032-4>
- Virtasalo, J. J., Österholm, P., Kotilainen, A. T., & Åström, M. E. (2020). Enrichment of trace metals from acid sulfate soils in sediments of the Kvarken Archipelago, Eastern Gulf of Bothnia, Baltic Sea. *Biogeosciences*, 17, 6097–6113. <https://doi.org/10.5194/bg-17-6097-2020>
- Vithana, C. L., Sullivan, L. A., Burton, E. D., & Bush, R. T. (2015). Stability of schwertmannite and jarosite in an acidic landscape: Prolonged field incubation. *Geoderma*, 239–240, 47–57. <https://doi.org/10.1016/j.geoderma.2014.09.022>
- Wang, M., Wang, L., Shi, H., Liu, Y., & Chen, S. (2021). Soil bacteria, genes, and metabolites stimulated during sulfur cycling and cadmium mobilization under sodium sulfate stress. *Environmental Research*, 201, 111599. <https://doi.org/10.1016/j.envres.2021.111599>
- Warren, I. H. (1956). The generation of sulphuric acid from pyrite bypressure leachin. *Australian Journal of Applied Science*, 7, 346–358.
- Whaley-Martin, K., Jessen, G. L., Nelson, T. C., Mori, J. F., Apte, S., Jarolimiek, C., & Warren, L. A. (2019). The potential role of *Halothiobacillus* spp. in sulfur oxidation and acid generation in circum-neutral mine tailings reservoirs. *Frontiers in Microbiology*, 10, 297. <https://doi.org/10.3389/fmicb.2019.00297>
- Wickham, H., Averick, M., Bryan, J., Chang, W., McGowan, L., François, R., Grolemond, G., Hayes, A., Henry, L., Hester, J., Kuhn, M., Pedersen, T., Miller, E., Bache, S., Müller, K., Ooms, J., Robinson, D., Seidel, D., Spinu, V., ... Yutani, H. (2019). Welcome to the Tidyverse. *Journal of Open Source Software*, 4(43), 1686. <https://doi.org/10.21105/joss.01686>
- Wiklander, L., Hallgren, G., & Jonsson, E. (1950). Studies on gytjtja soils III. Rate of sulfur oxidation. *Annals of the Royal Agricultural College of Sweden*, 17, 425–440.
- Williams, C., Macalady, J., & Grettenberger, C. (2023). Metagenome-assembled genomes from Appalachian acid mine drainage sites. *Microbiology Resource Announcements*, 12, e01280-22. <https://doi.org/10.1128/mra.01280-22>
- Wu, X., Wong, Z. L., Sten, P., Engblom, S., Österholm, P., & Dopson, M. (2013). Microbial community potentially responsible for acid and metal release from an Ostrobothnian acid sulfate soil. *FEMS Microbiology Ecology*, 84, 555–563. <https://doi.org/10.1111/1574-6941.12084>
- Xia, Y., Wang, Y., Wang, Y., Chin, F. Y. L., & Zhang, T. (2016). Cellular adhesiveness and cellulolytic capacity in *Anaerolineae* revealed by omics-based genome interpretation. *Biotechnology for Biofuels*, 9, 111. <https://doi.org/10.1186/s13068-016-0524-z>
- Xu, Y., Liao, Y., Lin, Z., Lin, J., Li, Q., Lin, J., & Jin, Z. (2019). Precipitation of calcium sulfate dihydrate in the presence of fulvic acid and magnesium ion. *Chemical Engineering Journal*, 361, 1078–1088. <https://doi.org/10.1016/j.cej.2019.01.003>
- Yi, Q., You, F., Li, Z., Wu, S., Chan, T.-S., Lu, Y.-R., Thomsen, L., Wang, J., Ma, Y., Liu, Y., Robertson, L., Southam, G., & Huang, L. (2023). Elemental sulfur and organic matter amendment drive alkaline pH neutralization and mineral weathering in iron ore tailings through inducing sulfur oxidizing bacteria. *Environmental Science & Technology*, 57, 21744–21756. <https://doi.org/10.1021/acs.est.3c05749>
- Yu, C., Högfors-Rönholm, E., Stén, P., Engblom, S., & Åström, M. E. (2023). Iron-sulfur geochemistry and acidity retention in hydrologically active macropores of boreal acid sulfate soils: Effects of mitigation suspensions of fine-grained calcite and peat. *Science of the Total Environment*, 856, 159142. <https://doi.org/10.1016/j.scitotenv.2022.159142>
- Yu, C., Luong, N. T., Hefni, M. E., Song, Z., Högfors-Rönholm, E., Engblom, S., Xie, S., Chernikov, R., Broström, M., Boily, J.-F., & Åström, M. E. (2024). Storage and distribution of organic carbon and nutrients in acidic soils developed on sulfidic sediments: The roles of reactive iron and macropores. *Environmental Science & Technology*, 58, 9200–9212. <https://doi.org/10.1021/acs.est.3c11007>
- Yu, C., Turner, S., Huotari, S., Chen, N., Shchukarev, A., Österholm, P., Lopez-Fernandez, M., Högfors-Rönholm, E., Sachpazidou, V., Mayanna, S., Hogmalm, K. J., Virtasalo, J. J., Boily, J.-F., Dopson, M., & Åström, M. E. (2024). Manganese cycling and transport in boreal estuaries impacted by acidic Mn-rich drainage. *Geochimica et Cosmochimica Acta*, 365, 136–157. <https://doi.org/10.1016/j.gca.2023.12.004>
- Yu, C., Virtasalo, J. J., Karlsson, T., Peltola, P., Österholm, P., Burton, E. D., Arppe, L., Hogmalm, J. K., Ojala, A. E. K., & Åström, M. E. (2015). Iron behavior in a northern estuary: Large pools of non-sulfidized Fe(II) associated with organic matter. *Chemical Geology*, 413, 73–85. <https://doi.org/10.1016/j.chemgeo.2015.08.013>
- Zachara, J. M., Kukkadapu, R. K., Fredrickson, J. K., Gorby, Y. A., & Smith, S. C. (2002). Biomineralization of poorly crystalline Fe(III) oxides by dissimilatory metal reducing bacteria (DMRB). *Geomicrobiology Journal*, 19, 179–207. <https://doi.org/10.1080/01490450252864271>
- Zhu, M., Wu, J., Yang, Z., Zhu, Y., Rong, Q., & Wen, Q. (2023). Effect of the textures and particle sizes of limestone on the quicklime reaction activity. *Minerals*, 13, 1201. <https://doi.org/10.3390/min13091201>

SUPPORTING INFORMATION

Additional supporting information can be found online in the Supporting Information section at the end of this article.

How to cite this article: Kononova, L., Johnson, A., Engblom, S., Stén, P., Yu, C., Österholm, P., Kessler, V., Seisenbaeva, G., Dopson, M., Åström, M., & Högfors-Rönholm, E. (2025). Geochemical and microbial responses to limestone and peat treatment of incubated hypermonosulfidic sediments. *European Journal of Soil Science*, 76(1), e70024. <https://doi.org/10.1111/ejss.70024>